

Duck Traps: Two-dimensional Critical Manifolds in Planar Systems

Christian Kuehn*and Christian Münch†

November 6, 2018

Abstract

In this work we consider two-dimensional critical manifolds in planar fast-slow systems near fold and so-called canard (=“duck”) points. These higher-dimension, and lower-codimension, situation is directly motivated by the case of hysteresis operators limiting onto fast-slow systems as well as by systems with constraints. We use geometric desingularization via blow-up to investigate two situations for the slow flow: generic fold (or jump) points, and canards in one-parameter families. We directly prove that the fold case is analogous to the classical fold involving a one-dimensional critical manifold. However, for the canard case, considerable differences and difficulties appear. Orbits can get trapped in the two-dimensional manifold after a canard-like passage thereby preventing small-amplitude oscillations generated by the singular Hopf bifurcation occurring in the classical canard case, as well as certain jump escapes.

Keywords: Multiple time scale dynamics; fast-slow systems; fold point; canard; piecewise smooth system; blow-up method

1 Introduction

In this introductory section, we are going to explain the main concepts of fast-slow systems, non-hyperbolicity and the blow-up technique. Furthermore, we are going to motivate codimension zero critical manifolds as considered in this work arising from hysteresis operators. Then we present our main results on an informal level. A typical planar fast-slow system

*CONTACT Christian Kuehn. Email: ckuehn@ma.tum.de

†CONTACT Christian Münch. Email: christian.muench@ma.tum.de

takes the form

$$\varepsilon \frac{dx}{d\tau} = \varepsilon \dot{x} = f(x, y, \varepsilon), \quad (1.1)$$

$$\frac{dy}{d\tau} = \dot{y} = g(x, y, \varepsilon), \quad (1.2)$$

for $x \in \mathbb{R}^m, y \in \mathbb{R}^n$, with a small parameter $0 < \varepsilon \ll 1$ and given initial conditions. In the classical case, f, g are assumed to be sufficiently smooth functions [6, 7, 11]. Later on, we are going to restrict attention to the piecewise smooth case. Since ε is small, one can consider first the singular limit $\varepsilon = 0$ in (1.1)–(1.2), which gives the reduced system (or slow subsystem)

$$0 = f(x, y, 0), \quad (1.3)$$

$$\dot{y} = g(x, y, 0), \quad (1.4)$$

which is a differential-algebraic equation. Here, the critical manifold

$$\mathcal{C}_0 := \{(x, y) \in \mathbb{R}^{m+n} : f(x, y, 0) = 0\}$$

generically has codimension m , see (c) in Figure 1. Substituting the fast time scale $t := \tau/\varepsilon$ into (1.1)–(1.2) yields the system

$$x' = f(x, y, \varepsilon), \quad (1.5)$$

$$y' = \varepsilon g(x, y, \varepsilon), \quad (1.6)$$

and this time the limit $\varepsilon = 0$ takes the form of a parametrized differential equation, the layer problem (or fast subsystem)

$$x' = f(x, y, 0), \quad (1.7)$$

$$y' = 0. \quad (1.8)$$

Intuitively, we expect that a singular limit of solutions for (1.1)–(1.2), or equivalently (1.5)–(1.6), as $\varepsilon \rightarrow 0$ should qualitatively behave according to some weighted mixture between (1.3)–(1.4) and (1.7)–(1.8). For sufficiently smooth functions f, g , this is indeed the case. In particular, for sufficiently small $\varepsilon > 0$ and outside $\mathcal{O}(\varepsilon)$ -distance of the critical manifold $\{f(x, y, 0) = 0\}$, the solution of (1.5)–(1.6) is well approximated by the layer problem, i.e., the x -components evolve fast while the y -components remain almost constant. A subset $M \subset \mathcal{C}_0$ is called normally hyperbolic, if $D_x f(p, 0)$ is a hyperbolic matrix for all $p \in M$ [6, 7, 11]. In particular, an equilibrium (x_*, y_*) of (1.5)–(1.6) in \mathcal{C}_0 is normally hyperbolic if $D_x f(x_*, y_*, 0)$ has no eigenvalues with zero real parts. With this definition, in $\mathcal{O}(\varepsilon)$ -distance of any normally hyperbolic compact subset of the critical manifold, Fenichel

theory yields the existence of a perturbed invariant slow manifold, such that the system (1.5)–(1.6) restricted to this manifold behaves similar to the reduced flow [6], see also [7, 11, 17] for Fenichel theory and its broader context. Additionally, the slow manifold has the same stability properties as the critical manifold, i.e., it is attracting/repelling for solutions of (1.5)–(1.6) for different directions, in the same way as the original subset \mathcal{C}_0 was for the layer problem (1.7)–(1.8).

The situation gets more complicated if the critical manifold contains non-hyperbolic points. A very powerful tool to analyze the dynamics close to such points is the so-called blow-up technique used in several contexts in fast-slow systems [4, 5, 8, 11]. The idea is to transform the (extended) fast-slow system (1.5)–(1.6) given by

$$\begin{aligned}x' &= f(x, y, \varepsilon), \\y' &= \varepsilon g(x, y, \varepsilon), \\ \varepsilon' &= 0,\end{aligned}$$

in such a way, that a non-hyperbolic equilibrium point $(x_*, y_*, 0)$ is blown-up, e.g., to a whole sphere. Frequently, the resulting desingularized system contains only (partially) hyperbolic equilibria, which improves the situation dynamically, i.e., we have gained hyperbolicity. For illustration, let us consider the case $m = 1 = n$ (as applied in this work, see also [8, 1, 5]) and the polar blow-up of the system in case of a canard point. This system depends on an additional parameter λ , which we can also append via $\lambda' = 0$, and one is interested in the local dynamics around the equilibrium $(0, 0, 0, 0)$ (the canard point) for small ε and upon variation of λ . In particular, the system is blown-up to $(\bar{x}, \bar{y}, \bar{\varepsilon}, \bar{\lambda}, \bar{r}) \in \mathbb{S}^2 \times [-\mu, \mu] \times [0, \rho]$ by the transformation Ψ , which is defined by

$$x = \bar{r}\bar{x}, \quad y = \bar{r}^2\bar{y}, \quad \varepsilon = \bar{r}^2\bar{\varepsilon}, \quad \lambda = \bar{r}\bar{\lambda}. \quad (1.9)$$

Here, for $\bar{r} = 0$ and all $\bar{\lambda} \in [-\mu, \mu]$, Ψ maps the sphere $\mathbb{S}^2 = \{\bar{x}^2 + \bar{y}^2 + \bar{\varepsilon}^2 = 1\}$ to the canard point $(0, 0, 0, 0)$, see (a) in Figure 1.

Typically, the dynamics for the blown-up system is analyzed in different (overlapping) directional charts. Fenichel theory can be applied in the regions, which correspond to parts far enough away from any non-hyperbolic point of (1.5)–(1.6), and here the dynamics is analyzed in directional charts corresponding to $\bar{y}, \bar{x} = \pm 1$, depending on the signs of x, y in these areas. For the canard point, we need one chart K_1 for the direction $\bar{y} = 1$. The corresponding transformation map Φ_1 is determined by

$$x = r_1 x_1, \quad y = r_1^2, \quad \varepsilon = r_1^2 \varepsilon_1, \quad \lambda = r_1 \lambda_1, \quad (1.10)$$

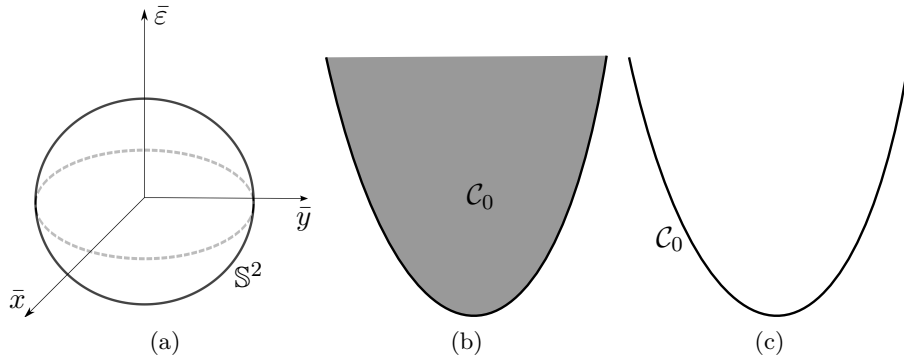


Figure 1: (a): Projection to $(\bar{x}, \bar{y}, \bar{\varepsilon})$ -coordinates of the reduced system $\bar{r} = 0$ of the weighted polar blow-up Ψ . The canard point $(0, 0, 0, 0)$ is blown-up to $\mathbb{S}^2 \times [-\mu, \mu]$. (b): Example of a critical manifold \mathcal{C}_0 (gray) with codimension zero in the plane $m = 1 = n$. (c): Example of a critical manifold \mathcal{C}_0 with codimension one in the plane $m = 1 = n$.

with domain

$$V_1 = (-x_{1,0}, x_{1,0}) \times [-\rho, \rho] \times [0, 1] \times (-\mu, \mu).$$

Here, $x_{1,0} > 0$ is chosen sufficiently large, and $\rho > 0, \mu > 0$ are chosen sufficiently small. That is, $\varepsilon \in [0, \varepsilon_0)$ with $\varepsilon_0 = \rho^2$. Chart K_1 is necessary to study (4.29)–(4.32) in sets of the form $\{(x, y) : y \in (\varepsilon, \rho^2], x \in (-x_{1,0}\sqrt{y}, x_{1,0}\sqrt{y})\}$. For $\varepsilon \in (0, \rho^2]$, we define

$$V_{1,\varepsilon} := \{(x_1, r_1, \varepsilon_1, \lambda_1) \in V_1 : r_1^2 \varepsilon_1 = \varepsilon\}.$$

The dynamics close to the equilibrium point is usually analyzed with help of a rescaling (or classical) chart K_2 , that is, with the directional chart corresponding to $\bar{\varepsilon} = 1$. In the canard case, the corresponding transformation map Φ_2 is determined by

$$x = r_2 x_2, \quad y = r_2^2 y_2, \quad \varepsilon = r_2^2, \quad \lambda = r_2 \lambda_2, \quad (1.11)$$

with domain

$$V_2 = D \times [0, \rho] \times (-\mu, \mu).$$

Here, D is a sufficiently large disc with center $(0, 0)$. Chart K_2 is applied to study the system in a neighbourhood of the origin of size $\mathcal{O}(\sqrt{\varepsilon})$ in x -direction and $\mathcal{O}(\varepsilon)$ in y -direction. For $\varepsilon \in (0, \rho^2]$, we define

$$V_{2,\varepsilon} := \{(x_2, y_2, r_2, \lambda_2) \in V_2 : r_2^2 = \varepsilon\}.$$

The analysis will be carried out in these sets in the blow-up, and it is helpful to already introduce two other sets (see also Figure 2):

Definition 1.1. For $\varepsilon \in (0, \rho^2]$ and $P_{(x,y)}$ the projection to (x, y) -coordinates we define the set

$$V_\varepsilon := P_{(x,y)}(\Phi_1(V_{1,\varepsilon})) \cup P_{(x,y)}(\Phi_2(V_{2,\varepsilon})).$$

Moreover, we define $V := V_{\varepsilon_0} = V_{\rho^2}$.

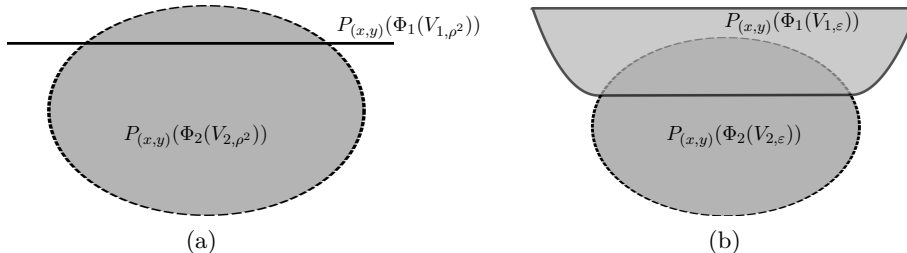


Figure 2: (a): Sketch of $V = V_{\rho^2}$. In particular, V is the union of the line $P_{(x,y)}(\Phi_1(V_{1,\rho^2})) = \{(x, y) : y = \rho^2, x \in (-x_{1,0}\sqrt{y}, x_{1,0}\sqrt{y})\}$, and the ellipse $P_{(x,y)}(\Phi_2(V_{2,\rho^2}))$ (dashed gray) which has width of order $\mathcal{O}(\rho)$ and height of order $\mathcal{O}(\rho^2)$. (b): Sketch of V_ε for $\varepsilon \in (0, \rho^2)$. V_ε is the union of $P_{(x,y)}(\Phi_1(V_{1,\rho^2})) = \{(x, y) : y \in (\varepsilon, \rho^2], x \in (-x_{1,0}\sqrt{y}, x_{1,0}\sqrt{y})\}$ (solid light gray) and the ellipse $P_{(x,y)}(\Phi_2(V_{2,\rho^2}))$ (dashed dark gray) which has width of order $\mathcal{O}(\sqrt{\varepsilon})$ and height of order $\mathcal{O}(\varepsilon)$.

We also remark that for some problems, it requires more than one blow-up until all non-hyperbolic points (arising during the iterated blow-ups) have gained enough hyperbolicity. For the results in this work, one weighted polar blow-up as outlined above will be sufficient.

Different from the classical assumption, we analyze fast-slow systems with critical manifold of codimension zero for $m = 1 = n$, i.e. \mathcal{C}_0 has dimension two, see (b) in Figure 1. This implies that the non-linearity f is only piecewise smooth, yet our case is substantially different from other piecewise smooth fold cases (see e.g. [3, 10, 15]), where the critical manifold is less regular but still of dimension one. For our case of a dimension two critical manifold, we have to carefully analyze the (local) dynamics of system (1.5)–(1.6) on either side of the particular manifold where f is not differentiable. The equilibrium point, which is non-hyperbolic for the smooth system, will be located in the separating manifold for the two smooth regions. It turns out, that the same blow-up as for the smooth system can yield the desired results, but interesting additional and novel phenomena are observed.

In particular, the curvature of the function g , which determines the slow flow, is crucial now. More precisely, if $x \mapsto g(x, y, 0)$, $(x, y) \in \mathcal{C}_0$ is not one-to-one, then the fast-slow system has several equilibria within \mathcal{C}_0 . Hence, different from the classical case, higher order terms of f and g become relevant for the local analysis around the non-hyperbolic equilibrium. Fast-slow systems with critical manifold of codimension zero are relevant in several applications. Amongst others, the coupling of (systems) of ordinary differential equations (ODEs) or partial differential equations (PDEs) and a hysteresis operator are often approximated by the singular limit of fast-slow systems, see e.g. [12, 14, 13]. A particular subclass of interesting scalar hysteresis operators are so-called generalized play operators [2, 16]. Given two increasing and (piecewise) smooth functions

$$L, U : \mathbb{R} \rightarrow \mathbb{R}, \quad L < U,$$

the corresponding generalized play operator \mathcal{P} maps time-continuous functions $y = y(t)$ to time-continuous functions $\mathcal{P}[y]$. Here, $\mathcal{P}[y]$ remains constant while $(y, \mathcal{P}[y])$ is located between the graphs $(y, U(y))$ and $(y, L(y))$. Once $\mathcal{P}[y] = L(y)$, so that the right curve $(y, L(y))$ is touched by $(y, \mathcal{P}[y])$ in phase space, then $\mathcal{P}[y]$ increases according to $\mathcal{P}[y] = L(y)$ as long as y is monotone increasing. Similarly, $\mathcal{P}[y] = U(y)$ holds as long as y is decreasing once $(y, \mathcal{P}[y])$ touches the left graph $(y, U(y))$. In other words, $\mathcal{P}[y]$ remains constant if located strictly between the graphs of L and U , and otherwise moves on the graphs, see (a) in Figure 3.

Finally, $L(y) \leq \mathcal{P}[y] \leq U(y)$ holds at all times. In particular, a prescribed fixed initial value $z_0 \in \mathbb{R}$, which can be located outside of $[L(y(0)), U(y(0))]$, is instantaneously projected to $[L(y(0)), U(y(0))]$ according to

$$\mathcal{P}[y](0) = \min\{\max\{L(y(0)), z_0\}, U(y(0))\}.$$

For the approximation by fast-slow systems, the non-linearity f which determines the fast flow x is therefore chosen such that its sign is negative for input parameters above the graph $(y, U(y))$ and positive below $(y, L(y))$, so that the fast flow is directed towards the area between both graphs. Note that $x(0) = z_0 \in \mathbb{R}$ can be located outside of $[L(y(0)), U(y(0))]$. Choosing $f = 0$ between $(y, U(y))$ and $(y, L(y))$, it turns out that the fast variable x tends to $\mathcal{P}[y]$ in the singular limit $\varepsilon \rightarrow 0$, while y still solves the slow equation. In particular, the two-dimensional area between the graphs of L and U is the critical manifold of the approximating fast-slow system, i.e., it has codimension zero. Note that in order to obtain interesting long-term effects in this setting, one has to allow time-dependent g , since $\mathcal{P}[y]$ is unchanged while y remains constant. However, before considering non-autonomous

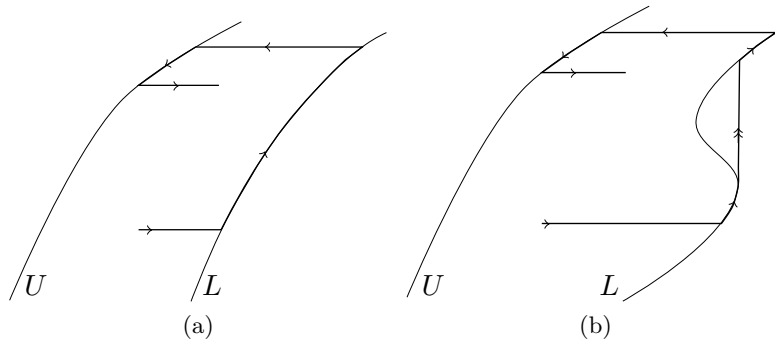


Figure 3: (a): Typical trajectory $(y, \mathcal{P}[y])$ in phase space of a classical generalized play operator, which is defined by two monotone increasing curves L and U . (b): Situation if one boundary curve (here L) contains a fold point. In particular, L is not monotone increasing. The solution behaves as a trajectory of a classical generalized play operator until it reaches the fold point. Then it jumps up, similar as trajectories of a relay operator, until it hits the graph of L again. Afterward, the solution continues as a trajectory of a classical generalized play operator.

systems, it is crucial to understand the dynamics of the autonomous system (1.5)–(1.6) first. If one drops the assumption that U and L have to be monotone increasing, then a non-hyperbolic point such as a fold can be generically located on e.g. L (or U). In this case, with ε small, some trajectories of the approximating fast-slow system, follow $(y, L(y))$ in (y, x) -phase space according to the slow dynamics up to the fold point and then jump upwards according to the fast dynamics until eventually arriving at a point on the graph $(y, L(y))$ again, see (b) in Figure 3.

In this work, we restrict to the local dynamics around one boundary curve of the critical manifold (i.e., we select U or L) which acts attracting from one side. In particular, we analyze the local dynamics of the corresponding system if this curve contains a non-hyperbolic point, as in (b) in Figure 3.

The outline of this work is the following. In Section 2, we analyze the analogous behaviour to a so-called fold singularity in the codimension zero setting. In particular, we extend the critical manifold

$$\mathcal{C}_\partial := \{(x, y) \in \mathbb{R}^2 : y = x^2\}$$

to one side by replacing $f(x, y) = -y + x^2$ by zero on one side of \mathcal{C}_∂ . This yields a fast-slow system with critical manifold

$$\mathcal{C}_0 = \{(x, y) \in \mathbb{R}^2 : y \geq x^2\},$$

which has the classical form of a system with a fold singularity, but only from one side. In Theorem 2.1 we restate a classical result for the local dynamics of the slow flow close to the fold point, see [5, 8, 9, 11]. In Theorem 2.2, we prove that this classical result still applies in the codimension zero setting, by proving that the set $\mathbb{R}^2 \setminus \mathcal{C}_0$ is invariant. In particular, Theorem 2.2 also applies if $f(x, y)$ is not replaced by the zero function in \mathcal{C}_0 , but by any other function $h(x, y)$. The result for $h = 0$ is summarized in Corollary 2.4.

In Sections 3–4, we analyze the analogous case to a canard singularity in the codimension zero setting, which turns out to be far more difficult. Again, $f(x, y) = -y + x^2$ is set to zero on one side of \mathcal{C}_∂ , and the resulting fast-slow system has again critical manifold $\mathcal{C}_0 = \{(x, y) \in \mathbb{R}^2 : y \geq x^2\}$. The function g this time takes the form

$$g = xg_1 - \lambda g_2 + yg_3, \quad \text{with} \quad g_1, g_2 = 1 + \mathcal{O}(x, y, \lambda),$$

and we want to analyze the fast-slow system for $\varepsilon > 0$ and for different parameters λ . In Section 3, we restate the results for the classical planar canard case [8, 9]. Section 4 contains our main results on the dynamics within the small neighbourhood V of the equilibrium point $(0, 0) \in \mathcal{C}_\partial$ for $\lambda = 0$. We write $p_e = p_e(\lambda)$ for the (perturbed) equilibrium. In Theorem 4.2, we prove the existence of two critical values λ_H, λ_c and a branch of equilibria in \mathcal{C}_0 emanating from p_e , such that all trajectories starting on the left side of a small neighbourhood $U^0 = U^0(\lambda, \varepsilon)$ around this branch leave the critical manifold, re-enter it to the right of U^0 but close to p_e , and leave V in \mathcal{C}_0 , provided that $-\lambda_0 < \lambda < \lambda_H$. For $-\lambda_0 < \lambda < \lambda_*$, $\lambda_* \in (\lambda_H, \lambda_c)$, this neighbourhood U^0 around the graph $(x, u_e(x))$ of roots of $g(\cdot, \cdot, \lambda)$ has width $\mathcal{O}(\varepsilon + \sqrt{\varepsilon}\lambda)$ in $V_{2,\varepsilon}$ and respectively $\mathcal{O}((u_e(x))^2 + \lambda u_e(x))$ for $(x, u_e(x)) \in V_{1,\varepsilon}$. For $\lambda_* < \lambda < \lambda_0$, U^0 it has width $\mathcal{O}(\varepsilon^{3/2} + \sqrt{\varepsilon}\lambda)$ in $V_{2,\varepsilon}$ and respectively $\mathcal{O}((u_e(x))^2 + \lambda u_e(x))$ for $(x, u_e(x)) \in V_{1,\varepsilon}$. The result follows since p_e is attracting in the classical case for all $-\lambda_0 < \lambda < \lambda_H$. Moreover, we prove that a maximal canard solution exists just as in the classical case if and only if $\lambda = \lambda_c$.

In Theorem 4.3, we show that stable half orbits below the parabola \mathcal{C}_∂ occur as λ passes through λ_H . In particular, trajectories starting left of U^0 in \mathcal{C}_0 which exit the critical manifold outside of such a half orbit, are attracted to the half orbit from the outside and re-enter \mathcal{C}_0 to the right of it before they leave V in \mathcal{C}_0 . Similarly, trajectories which reach the parabola inside the half orbit stay there as long as they are located outside of the critical manifold, and re-enter \mathcal{C}_0 inside the half orbit before they leave V in \mathcal{C}_0 . As the periodic orbits in the classical setting, also the half orbits get larger as $\lambda > \lambda_H$ increases up to a critical value $\lambda_{sc} < \lambda_c$, which is close

to the maximal canard value, see Figure 6 for a numerical example. Yet, note carefully that these (non-maximal) canards essentially get trapped in \mathcal{C}_0 showing a very significant difference to the classical case.

Finally, in Theorem 4.5, we analyze the behaviour for large values $\lambda_c < \lambda < \lambda_0$. In particular, we prove the existence of a vertical line P_c in (x, y) -space, such that all solutions starting to the left of P_c leave the neighbourhood V below the critical manifold. All solutions starting in $\mathcal{C}_0 \setminus U^0$ and to the right of P_c leave V in \mathcal{C}_0 and right of the branch of U^0 , see Figure 7. Hence, there is again a trapping effect for part of the orbits.

In summary, our results provide a complete characterization of the local dynamics around fold and canard points in planar fast-slow systems $m = 1 = n$, when the critical manifold \mathcal{C}_0 has codimension zero. Furthermore, we develop a refinement of the blow-up near folds applicable to higher-codimension situations, which may also appear in a wide variety of other contexts, not only for hysteresis operators.

2 Blow-up technique for the fold

2.1 The classical case

The classical fast-slow system for the fold normal form is given by

$$x' = -y + x^2, \quad (2.12)$$

$$y' = -\varepsilon. \quad (2.13)$$

The critical manifold for this system is given by the parabola

$$\mathcal{C}_\partial := \{(x, y) \in \mathbb{R}^2 : y = x^2\},$$

i.e. by a one-dimensional manifold in a two-dimensional dynamical system. We also introduce the attracting and repelling branch

$$\mathcal{C}_0^a := \mathcal{C}_\partial \cap (\mathbb{R}^- \times \mathbb{R}), \quad \mathcal{C}_0^r := \mathcal{C}_\partial \cap (\mathbb{R}^+ \times \mathbb{R}).$$

System (2.12)–(2.13), and specifically its dynamics around the non-hyperbolic fold point $(0, 0)$, has been analyzed in [8]. In particular, a blow-up of the fold was applied to study the local behaviour around this point. The main result [8, Theorem 2.1] is the following: Let $\rho > 0$ be chosen small enough and consider sections

$$\Delta_{\text{in}} := \{(x, \rho^2) : x \in J\}, \quad \Delta_{\text{out}} := \{(\rho, y) : y \in \mathbb{R}\}$$

for some suitable interval $J \subset \mathbb{R}$. Let $\Pi : \Delta_{\text{in}} \rightarrow \Delta_{\text{out}}$ be the transition map for the flow (2.12)–(2.13).

Theorem 2.1. *There exists $\varepsilon_0 > 0$ such that the following assertions hold for $\varepsilon \in (0, \varepsilon_0)$:*

(T1) *The attracting slow manifold $\mathcal{C}_\varepsilon^a$ passes through Δ_{out} at a point $(\rho, h(\varepsilon))$, where $h(\varepsilon) = \mathcal{O}\left(\varepsilon^{\frac{2}{3}}\right)$.*

(T2) *The transition map Π is a contraction with contraction rate $\mathcal{O}\left(e^{-\frac{c}{\varepsilon}}\right)$, where c is a positive constant.*

This result is shown by an appropriate blow-up transformation near the fold point. Three directional charts K_1 to K_3 are necessary to describe the behaviour of trajectories close to the origin. K_1 is determined by

$$x = r_1 x_1, \quad y = r_1^2, \quad \varepsilon = r_1^3 \varepsilon_1.$$

In the chart K_1 , the desingularized vector field (i.e. divided by r_1) reads

$$\begin{aligned} x_1' &= -1 + x_1^2 + \frac{1}{2} \varepsilon_1 x_1, \\ r_1' &= -\frac{1}{2} r_1 \varepsilon_1, \\ \varepsilon_1' &= \frac{3}{2} \varepsilon_1^2. \end{aligned}$$

Similarly, the rescaling chart K_2 is determined by

$$x = r_2 x_2, \quad y = r_2^2 y_2, \quad \varepsilon = r_2^3,$$

and the desingularized vector field (i.e. divided by r_2) reads

$$\begin{aligned} x_2' &= -y_2 + x_2^2, \\ y_2' &= -1, \\ \dot{r}_2 &= 0. \end{aligned}$$

Finally, K_3 is determined by

$$x = r_3, \quad y = r_3^2 y_3, \quad \varepsilon = r_3^3 \varepsilon_3,$$

and the desingularized vector field (i.e. divided by r_3) reads

$$\begin{aligned} r_3' &= r_3(-y_3 + 1), \\ y_3' &= -\varepsilon_3 - 2y_3(-y_3 + 1), \\ \varepsilon_3' &= -3\varepsilon_3(1 - y_3). \end{aligned}$$

2.2 Two-dimensional critical manifold

The situation is somewhat different to the classic fold if the critical manifold has codimension zero. Consider the fast-slow system

$$x' = \begin{cases} -y + x^2 & \text{for } y < x^2, \\ h(x, y) & \text{for } y \geq x^2, \end{cases} \quad (2.14)$$

$$y' = -\varepsilon. \quad (2.15)$$

For $h(x, y) = 0$, the critical manifold is given by $\mathcal{C}_0 = \{(x, y) \in \mathbb{R}^2 : y \geq x^2\}$. Moreover, for $h(x, y) = -y + x^2$, the critical manifold is given by $\mathcal{C}_\partial = \{(x, y) \in \mathbb{R}^2 : y = x^2\}$ as for the classical fold. In this case, system (2.14)–(2.15) has a non-hyperbolic equilibrium at $(0, 0)$, see Figure 4, and Theorem 2.1 applies.

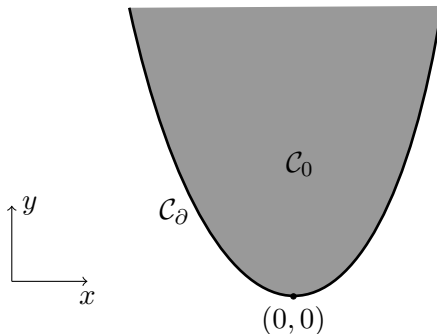


Figure 4:

The two-dimensional set \mathcal{C}_0 (gray) depicts the critical manifold for the case $h(x, y) = 0$. Its lower boundary \mathcal{C}_∂ represents the critical manifold for the classical case $h(x, y) = -y + x^2$. The fold point, which will later be a canard point in Sections 3–4, is located at $(0, 0)$.

We keep the notation \mathcal{C}_0 also for $h(x, y) \neq 0$. It turns out that Theorem 2.1 applies at least partly to the problem (2.14)–(2.15).

As in the previous section, let $\rho > 0$ be chosen small enough and consider sections

$$\tilde{\Delta}_{\text{in}} := \{(x, \rho^2) : x \in J\}, \quad \tilde{\Delta}_{\text{out}} := \{(\rho, y) : y \in (-\infty, \rho^2)\}$$

for some suitable interval $J \subset (-\infty, -\rho)$. Let $\tilde{\Pi} : \tilde{\Delta}_{\text{in}} \rightarrow \tilde{\Delta}_{\text{out}}$ be the transition map for the flow (2.14)–(2.15).

Theorem 2.2. *There exists $\varepsilon_0 > 0$ such that the following assertions hold for $\varepsilon \in (0, \varepsilon_0)$:*

$\tilde{\Pi} : \tilde{\Delta}_{\text{in}} \rightarrow \tilde{\Delta}_{\text{out}}$ is the restriction of the transition map Π from the previous section to the set $\tilde{\Delta}_{\text{in}}$.

(T1) The attracting slow manifold $\mathcal{C}_\varepsilon^a$ passes through $\tilde{\Delta}_{\text{out}}$ at a point $(\rho, h(\varepsilon))$, where $h(\varepsilon) = O\left(\varepsilon^{\frac{2}{3}}\right)$.

(T2) The transition map Π is a contraction with contraction rate $O\left(e^{-\frac{c}{\varepsilon}}\right)$, where c is a positive constant.

In order to prove Theorem 2.2 it is enough to show the following lemma:

Lemma 2.3. System (2.14)–(2.15), transformed into the different charts K_1 – K_3 , leaves the set $\mathbb{R}^2 \setminus \mathcal{C}_0$ invariant. In particular, solution trajectories which start in $\mathbb{R}^2 \setminus \mathcal{C}_0$ never enter \mathcal{C}_0 .

Proof. We show that the dynamics of trajectories starting in the left (x, y) -half plane, and close to but outside of \mathcal{C}_0 , is independent of the particular vector field $h(x, y)$. In particular, for $\varepsilon > 0$, each trajectory $(x_\varepsilon, y_\varepsilon)$ starting in $\mathbb{R}^2 \setminus \mathcal{C}_0$ remains there. Since the blow-up technique in this case delivers the same results as for problem (2.14)–(2.15) with $h(x, y) = -y + x^2$ which has been analyzed in [8], we only have to transform (2.14)–(2.15) with general h into the single charts and make sure that the critical set \mathcal{C}_0 remains untouched. In chart K_1 , the desingularized vector field (i.e. divided by r_1) reads

$$x'_1 = \begin{cases} -1 + x_1^2 + \frac{1}{2}\varepsilon_1 x_1, & \text{for } 1 < |x_1|, \\ \frac{1}{r_1}h(r_1 x_1, r_1^2) + \frac{1}{2}\varepsilon_1 x_1, & \text{for } 1 \geq |x_1|, \end{cases} \quad (2.16)$$

$$r'_1 = -\frac{1}{2}r_1\varepsilon_1, \quad (2.17)$$

$$\varepsilon'_1 = \frac{3}{2}\varepsilon_1^2. \quad (2.18)$$

In chart K_2 , the desingularized vector field (i.e. divided by r_2) reads

$$x'_2 = \begin{cases} -y_2 + x_2^2, & \text{for } y_2 < x_2^2, \\ \frac{1}{r_2}h(r_2 x_2, r_2^2 y_2), & \text{for } y_2 \geq x_2^2, \end{cases} \quad (2.19)$$

$$y'_2 = -1, \quad (2.20)$$

$$\dot{r}_2 = 0. \quad (2.21)$$

Finally, in chart K_3 , the desingularized vector field (i.e. divided by r_3) reads

$$r'_3 = \begin{cases} r_3(-y_3 + 1), & \text{for } y_3 < 1, \\ \frac{1}{r_3}h(r_3, r_3^2 y_3), & \text{for } y_3 \geq 1, \end{cases} \quad (2.22)$$

$$y'_3 = \begin{cases} -\varepsilon_3 - 2y_3(-y_3 + 1), & \text{for } y_3 < 1, \\ -\varepsilon_3 - 2y_3 \frac{1}{r_3}h(r_3, r_3^2 y_3), & \text{for } y_3 \geq 1, \end{cases} \quad (2.23)$$

$$\varepsilon'_3 = \begin{cases} -3\varepsilon_3(1 - y_3), & \text{for } y_3 < 1, \\ -3\varepsilon_3 \frac{1}{r_3}h(r_3, r_3^2 y_3), & \text{for } y_3 \geq 1. \end{cases} \quad (2.24)$$

Note that the functions $\frac{1}{r_1}h(r_1x_1, r_1^2)$, $\frac{1}{r_2}h(r_2x_2, r_2^2y_2)$ and $\frac{1}{r_3}h(r_3, r_3^2y_3)$ are in general not bounded for $r_3 \rightarrow 0$. Nevertheless, we are only interested in the regions $\{1 < |x_1|\}$, $\{y_2 < x_2^2\}$ and $\{y_3 < 1\}$. In particular, we prove that no trajectory starting outside the blown-up sets of \mathcal{C}_0 , i.e. outside the sets $\{1 \geq |x_1|\}$, $\{y_2 \geq x_2^2\}$ and $\{y_3 \geq 1\}$, reaches them. Hence, we do not have to consider the particular dynamics in these latter cases. For $h(x, y) = 0$, there is no problem at all. Since $\varepsilon'_1 > 0$, the set $\{1 < |x_1|\}$ is invariant under (2.16)–(2.18). Transformed into the chart K_2 , the set $\{1 < |x_1|\}$ is given by $\{y_2 < x_2^2\}$. By [8, Proposition 2.3 2,5 and Proposition 2.6 5] each trajectory starting in the set $\{y_2 < x_2^2\}$ remains in this set. By [8, Proposition 2.3 1 and 5], the y_2 -component of each such trajectory is asymptotic to some $y_r < 0$ and x_2 gets positive at some time. The transformation $y_3 = y_2x_2^{-2} < 0$ [8, Lemma 2.2] implies that we arrive in the set $\{y_3 < 1\}$. Finally, [8, Proposition 2.11] proves that we remain in this set. Hence, the main result [8, Theorem 2.1] applies for all solutions $(x_\varepsilon, y_\varepsilon)$ of (2.14)–(2.15) which start in $(\mathbb{R}^- \times \mathbb{R}) \setminus \mathcal{C}_0$. \square

Note that Lemma 2.3 determines the whole flow near the fold point for the particular case $h(x, y) = 0$. Indeed, for $h(x, y) = 0$, each trajectory starting at a point $(x_\varepsilon(0), y_\varepsilon(0)) \in \mathcal{C}_0 \cap (\mathbb{R}^- \times \mathbb{R})$ enters the set $(\mathbb{R}^- \times \mathbb{R}) \setminus \mathcal{C}_0$ at $(x_\varepsilon(0), x_\varepsilon(0)^2)$ and then remains in this set. Also for starting points $(x_\varepsilon(0), y_\varepsilon(0)) \in \mathcal{C}_0 \cap (\mathbb{R}^+ \times \mathbb{R})$, the trajectory $(x_\varepsilon, y_\varepsilon)$ leaves the set \mathcal{C}_0 at $(x_\varepsilon(0), x_\varepsilon(0)^2)$ and, since it does not pass close to the fold point, classical theory can be applied for the further analysis. In particular, from $(x_\varepsilon(0), x_\varepsilon(0)^2)$, in first order approximation, the trajectory continues horizontally to the right on the line $\{(x, x_\varepsilon(0)^2) : x \geq x_\varepsilon(0)\}$. We summarize this special case in the following corollary:

Corollary 2.4. Let the assumptions of Theorem 2.2 hold and fix $\varepsilon \in (0, \varepsilon_0]$. Consider system (2.14)–(2.15) with $h(x, y) = 0$.

Each solution with $(x_\varepsilon(0), y_\varepsilon(0)) \in \mathcal{C}_0$ moves vertically downwards in (x, y) -phase space and enters the invariant set $\mathbb{R}^2 \setminus \mathcal{C}_0$ at $(x_\varepsilon(0), x_\varepsilon(0)^2)$.

For $x_\varepsilon(0) < 0$, the trajectory then stays $\mathcal{O}(\varepsilon)$ -close to the set \mathcal{C}_∂ until it reaches a point in Δ_{in} , from where Theorem 2.2 applies.

For $x_\varepsilon(0) > 0$, from $(x_\varepsilon(0), x_\varepsilon(0)^2)$, the trajectory is approximated to leading order by the fast subsystem and continues toward the right in (x, y) -phase space.

3 The classical canard case

The normal form of a canard point is given by [11, 8, 9]

$$x' = -y + x^2, \quad (3.25)$$

$$y' = \varepsilon g(x, y, \lambda), \quad (3.26)$$

$$\varepsilon' = 0, \quad (3.27)$$

$$\lambda' = 0, \quad (3.28)$$

where $g = xg_1 - \lambda g_2 + yg_3$ is C^r -smooth for $r \geq 3$, $g_i = g_i(x, y, \lambda)$ for $i = 1, 2, 3$, and with $g_1, g_2 = 1 + \mathcal{O}(x, y, \lambda)$. We denote $a_1 = \partial_x g_1(0, 0, 0)$, $a_2 = g_3(0, 0, 0)$ and assume $a_1, a_2 > 0$. Moreover, $\varepsilon \in (0, \varepsilon_0]$ and $\lambda \in [-\lambda_0, \lambda_0]$ for certain values $\varepsilon_0, \lambda_0 > 0$. As for the classical fold, all points of the one-dimensional critical manifold $\mathcal{C}_\partial = \{(x, y) : y = x^2\}$ are normally hyperbolic, except for the canard point at the origin. While classical Fenichel theory can be applied near the hyperbolic subset of the critical manifold in order to determine the behaviour of the slow flow of (3.25)–(3.28), the blow-up (1.9) of the origin with directional charts (1.10)–(1.11) yields the corresponding results for the flow close to the canard point. The main results are the following:

Theorem 3.1. [9, Theorems 3.1–3.2] *Suppose ε_0, λ_0 are sufficiently small and consider $V = V_{\varepsilon_0}$ as defined in Definition 1.1. Then for all fixed $\varepsilon \in (0, \varepsilon_0]$, system (3.25)–(3.28) has exactly one equilibrium $p_e \in V$, which converges to the canard point as $(\varepsilon, \lambda) \rightarrow 0$. Furthermore, there exists a curve $\lambda_H(\sqrt{\varepsilon}) = -\frac{a_2}{2}\varepsilon + \mathcal{O}(\varepsilon^{\frac{3}{2}})$ such that p_e is stable for $\lambda < \lambda_H(\sqrt{\varepsilon})$ and loses stability through a Hopf bifurcation as λ passes through $\lambda_H(\sqrt{\varepsilon})$. Moreover, there exists a function smooth in $\sqrt{\varepsilon}$ given by*

$$\lambda_c(\sqrt{\varepsilon}) = -\left(\frac{a_2}{2} + \frac{-2a_1 - 2a_2}{8}\right)\varepsilon + \mathcal{O}(\varepsilon^{3/2}) = \frac{a_1 - a_2}{4}\varepsilon + \mathcal{O}(\varepsilon^{3/2}),$$

such that the attracting slow manifold $\mathcal{C}_\varepsilon^a$ connects to the repelling slow manifold $\mathcal{C}_\varepsilon^r$ if and only if $\lambda = \lambda_c(\sqrt{\varepsilon})$.

Theorem 3.2. [9, Theorems 4.1] *Suppose ε_0, λ_0 are sufficiently small and consider $V = V_{\varepsilon_0}$ as defined in Definition 1.1. Fix $\varepsilon \in (0, \varepsilon_0]$. Then the following statements hold:*

(i) *For $\lambda \in (-\lambda_0, \lambda_H(\sqrt{\varepsilon})]$ all orbits starting in V converge to p_e or leave V .*

(ii) *There exists a curve $\lambda = \lambda_{sc}(\sqrt{\varepsilon})$ and a constant $K > 0$, with*

$$0 < \lambda_c(\sqrt{\varepsilon}) - \lambda_{sc}(\sqrt{\varepsilon}) = \mathcal{O}(e^{-\frac{K}{\varepsilon}}),$$

such that for each $\lambda \in (\lambda_H(\sqrt{\varepsilon}), \lambda_{sc}(\sqrt{\varepsilon}))$ the system (3.25)–(3.28) has a unique attracting limit cycle $\Gamma_{(\lambda, \varepsilon)}$ contained in V . All orbits starting in V , except for p_e , either leave V or are attracted to $\Gamma_{(\lambda, \varepsilon)}$.

(iii) For $\lambda \in (\lambda_{sc}, \lambda_0]$ all orbits starting in V , except for p_e , leave V .

4 Introduction to the canard case

As for the fold, we now consider a two-dimensional critical manifold. While the dynamics for the fold remained relatively simple, more involved phenomena appear in the canard case. Consider the following fast-slow system:

$$x' = \begin{cases} -y + x^2 & \text{for } y < x^2, \\ 0 & \text{for } y \geq x^2, \end{cases} \quad (4.29)$$

$$y' = \varepsilon g(x, y, \lambda), \quad (4.30)$$

$$\varepsilon' = 0, \quad (4.31)$$

$$\lambda' = 0, \quad (4.32)$$

where again $g = xg_1 - \lambda g_2 + yg_3$ is C^r -smooth for $r \geq 3$, $g_i = g_i(x, y, \lambda)$ for $i = 1, \dots, 3$, and with $g_1, g_2 = 1 + \mathcal{O}(x, y, \lambda)$. Also in this case we denote $a_1 = \partial_x g_1(0, 0, 0)$, $a_2 = g_3(0, 0, 0)$ and assume $a_1, a_2 > 0$. Again, $\varepsilon \in (0, \varepsilon_0]$ and $\lambda \in [-\lambda_0, \lambda_0]$ for certain values $\varepsilon_0, \lambda_0 > 0$. The critical manifold is given by the two-dimensional set $\mathcal{C}_0 = \{(x, y) : y \geq x^2\}$, with lower boundary $\mathcal{C}_\partial = \{(x, y) : y = x^2\}$, see Figure 5.

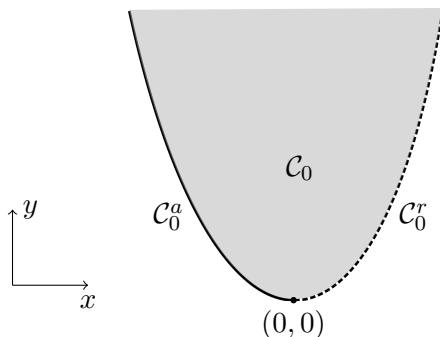


Figure 5:

The two-dimensional critical manifold $\mathcal{C}_0 = \{(x, y) \in \mathbb{R}^2 : y \geq x^2\}$ is depicted in gray. Its lower boundary \mathcal{C}_∂ is divided into the attracting branch $\mathcal{C}_0^a = \{(x, y) \in \mathbb{R}^- \times \mathbb{R} : y = x^2\}$ (solid black) and the repelling branch $\mathcal{C}_0^r = \{(x, y) \in \mathbb{R}^+ \times \mathbb{R} : y = x^2\}$ (dashed black). The canard point is located at $(0, 0)$.

Definition 4.1. In the following, we will frequently compare the relative position of two geometric sets $A, B \subset \mathbb{R}^2$ in the plane. We say that set A is (locally) located to the left of set B if for any $c \in \mathbb{R}$:

$$a \leq b, \quad \forall a \in A \cap \{(x, c) : x \in \mathbb{R}\}, b \in B \cap \{(x, c) : x \in \mathbb{R}\}.$$

In this case, B is (locally) located to the right of A . We say that A is totally located to the left of B if there exists x_{sep} such that $\{(x_{\text{sep}}, y) : y \in \mathbb{R}\}$ is locally located to the right of A and to the left of B . Similarly, we say that A lies (locally) below B if for any $c \in \mathbb{R}$:

$$a \leq b, \quad \forall a \in A \cap \{(c, y) : y \in \mathbb{R}\}, b \in B \cap \{(c, y) : y \in \mathbb{R}\}.$$

In this case, B is (locally) located above A . We say that A is totally located below B if there exists y_{sep} such that $\{(x, y_{\text{sep}}) : x \in \mathbb{R}\}$ is locally located above A and below B . If not further specified, we always mean the local definition, see Figure 6.

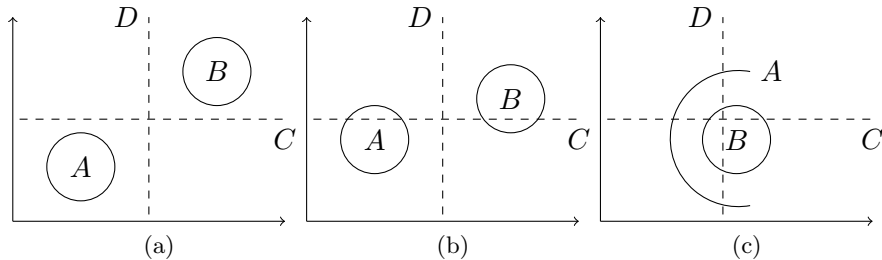


Figure 6: (a): Set A is locally located to the left and to the right of set B , since there exists no horizontal line which intersects both sets, i.e. the dashed horizontal line C separates A and B . Similarly, A is locally located above and below B , since there exists a separating vertical line D (dashed). However, totally, set A is located to the left of set B but not to the right, since A lies locally on the left side of the separating line D , while B lies locally on the right side of D . Similarly, set A is totally located below set B but not above. (b): Set A is locally located to the left of set B but not to the right, since for example the dashed line C intersects A and B and the x -component of all intersection points with A are strictly smaller than those with B . At the same time, A is still also totally located to the left of set B and not to the right, since A lies locally on the left side of the separating dashed line D , while B lies locally on the right side of D . As in (a), A is locally below and above B , since the vertical line D separates both sets. However, totally, A lies neither above nor below B , because there exists no horizontal line which lies locally above (below) A and below (above) B . (c): A lies locally to the left of B but not totally. At the same time, A lies neither locally nor totally below or above B .

For fixed ε and all $\lambda \in [-\lambda_0, \lambda_0]$, in contrast to the unique equilibrium p_e in Theorem 3.1, it turns out that system (4.29)–(4.32) has a unique curve $\Gamma_e = \Gamma_{e,\lambda}$ of equilibria emanating from p_e . This curve can locally be written as the graph of a function $(x, u_e(x))$. Since $x \mapsto u_e(x)$ is not necessarily one-to-one, the concrete curvature of g around Γ_e is crucial for the behaviour of system (4.29)–(4.32) close to Γ_e . Therefore, we consider a small neighbourhood $U^0 = U^0(\varepsilon, \lambda)$ around Γ_e . We will show the existence of some $\lambda_* \in (\lambda_H, \lambda_{sc})$ of the following kind: For $\lambda < \lambda_*$, U^0 can be chosen such that in $V_{2,\varepsilon}$, the left boundary of U^0 has distance of order $\mathcal{O}(\varepsilon + \sqrt{\varepsilon}\lambda)$ to Γ_e , while the right boundary of U^0 has distance of order $\mathcal{O}(\varepsilon^{3/2} + \sqrt{\varepsilon}\lambda)$ to Γ_e . For $\lambda > \lambda_*$, U^0 has width of order $\mathcal{O}(\varepsilon^{3/2} + \sqrt{\varepsilon}\lambda)$ in $V_{2,\varepsilon}$. For all $\lambda \in [-\lambda_0, \lambda_0]$, U^0 has width of order $\mathcal{O}((u_e(x))^2 + \lambda u_e(x))$ for $(x, u_e(x)) \in V_{1,\varepsilon}$, see Section 4.3 for the concrete definition. We will only consider the dynamics outside of U^0 . It will be crucial in several proofs that

the boundaries of U^0 are right-curved. If this is the case, we call U^0 right-curved. We also write U_0^-, U_0^+ for the left and right parts of $(V \cap \mathcal{C}_0) \setminus U^0$, see Section 4.3 for the concrete definition and compare Figure 7. Furthermore, the slow manifold is not longer given by a one-dimensional set, but has codimension zero just as the critical manifold. For this reason, we denote by $\mathcal{C}_\varepsilon^a$ and $\mathcal{C}_\varepsilon^r$ those parts of the attracting and repelling branches of the slow manifold of (3.25)–(3.28) which are located below \mathcal{C}_0 .

The adaption of Theorems 3.1–3.2 to the system (4.29)–(4.32) is the following, see also Figure 6:

Theorem 4.2. *Suppose ε_0, λ_0 are sufficiently small and consider $V = V_{\varepsilon_0}$ as defined in Definition 1.1. Then for all fixed $\varepsilon \in (0, \varepsilon_0]$, system (3.25)–(3.28) has exactly one equilibrium $p_e \in V \cap \mathcal{C}_\partial$, which converges to the canard point as $(\varepsilon, \lambda) \rightarrow 0$. Moreover, there exists a unique curve of equilibria $\Gamma_e = \Gamma_{e,\lambda} = \{(x, u_e(x))\}$ in $V \cap \mathcal{C}_0$, emanating from p_e , together with a right-curved neighbourhood $U^0 = U^0(\varepsilon, \lambda)$ around Γ_e . There exists a curve $\lambda_H(\sqrt{\varepsilon}) = -\frac{a_2}{2}\varepsilon + \mathcal{O}(\varepsilon^{\frac{3}{2}})$ such that for each value $\lambda \in (-\lambda_0, \lambda_H(\sqrt{\varepsilon})]$ all trajectories starting in $U_0^- \cup U_0^+$ leave V in U_0^+ . In particular, all solutions starting in U_0^- leave \mathcal{C}_0 , surround Γ_e close to p_e , return to \mathcal{C}_0 in U_0^+ and leave V in U_0^+ .*

There exists a smooth function

$$\lambda_c(\sqrt{\varepsilon}) = -\left(\frac{a_2}{2} + \frac{-2a_1 - 2a_2}{8}\right)\varepsilon + \mathcal{O}(\varepsilon^{3/2}) = \frac{a_1 - a_2}{4}\varepsilon + \mathcal{O}(\varepsilon^{3/2}),$$

such that $\mathcal{C}_\varepsilon^a$ connects to $\mathcal{C}_\varepsilon^r$ if and only if $\lambda = \lambda_c(\sqrt{\varepsilon})$. Moreover, $\mathcal{C}_\varepsilon^a$ and $\mathcal{C}_\varepsilon^r$ do not intersect \mathcal{C}_0 for $\lambda = \lambda_c(\sqrt{\varepsilon})$. In particular, maximal canard solutions exist if and only if $\lambda = \lambda_c(\sqrt{\varepsilon})$, and those solutions are located below \mathcal{C}_0 in V .

Theorem 3.2 claims the existence of limit cycles $\Gamma_{(\lambda,\varepsilon)}$ for each $\lambda \in (\lambda_H(\sqrt{\varepsilon}), \lambda_{sc}(\sqrt{\varepsilon}))$. In system (4.29)–(4.32), the same orbits are observed but only below \mathcal{C}_0 . Therefore, we write $\tilde{\Gamma}_{(\lambda,\varepsilon)} := (\mathbb{R}^2 \setminus \mathcal{C}_0) \cap \Gamma_{(\lambda,\varepsilon)}$ for the part of $\Gamma_{(\lambda,\varepsilon)}$ which is located below \mathcal{C}_0 . Since $x' = 0$ in \mathcal{C}_0 , each limit cycle of the classical canard system perturbs to the half orbit $\tilde{\Gamma}_{(\lambda,\varepsilon)}$ and its vertical extensions. More precisely, consider the left and right intersection points $p_- = (p_-^x, p_-^y)$ and $p_+ = (p_+^x, p_+^y)$ in $\Gamma_{(\lambda,\varepsilon)} \cap \mathcal{C}_\partial$, i.e. $p_-^x < p_+^x$. Moreover, denote by

$$P_- := \{(p_-^x, y) : y \in \mathbb{R}\}, \quad P_+ := \{(p_+^x, y) : y \in \mathbb{R}\} \quad (4.33)$$

the vertical extensions of $\Gamma_{(\lambda,\varepsilon)}$. Then in system (4.29)–(4.32), the limit cycle $\Gamma_{(\lambda,\varepsilon)}$ can be rediscovered in the form

$$\tilde{\Gamma}_{(\lambda,\varepsilon)} \cup [\mathcal{C}_0 \cap (P_- \cup P_+)].$$

The canard explosion for system (4.29)–(4.32) looks as follows, see also Figure 6:

Theorem 4.3. *Suppose ε_0, λ_0 are sufficiently small and consider $V = V_{\varepsilon_0}$ as defined in Definition 1.1. Fix $\varepsilon \in (0, \varepsilon_0]$ and consider the notation from Theorem 4.2. Then the following statements hold:*

(i) *For $\lambda \in (-\lambda_0, \lambda_H(\sqrt{\varepsilon})]$ all trajectories starting in $U_0^- \cup U_0^+$ leave V in U_0^+ . Moreover, all solutions starting in U_0^- leave \mathcal{C}_0 , surround Γ_e close to p_e , return to \mathcal{C}_0 in U_0^+ and leave V in U_0^+ .*

(ii) *There exists a curve $\lambda = \lambda_{sc}(\sqrt{\varepsilon})$ and a constant $K > 0$, with*

$$0 < \lambda_c(\sqrt{\varepsilon}) - \lambda_{sc}(\sqrt{\varepsilon}) = \mathcal{O}(e^{-\frac{K}{\varepsilon}}),$$

such that for each $\lambda \in (\lambda_H(\sqrt{\varepsilon}), \lambda_{sc}(\sqrt{\varepsilon}))$, system (4.29)–(4.32) has a unique attracting half cycle $\tilde{\Gamma}_{(\lambda, \varepsilon)}$ contained in $V \setminus \mathcal{C}_0$ and extended into \mathcal{C}_0 by $\mathcal{C}_0 \cap P_-$ and $\mathcal{C}_0 \cap P_+$. Moreover, all solutions of (4.29)–(4.32) starting in $V \setminus U^0$ and to the left of P_- or below $\tilde{\Gamma}_{(\lambda, \varepsilon)}$ leave V to the total right of P_+ . All trajectories starting in U_0^- and to the left of P_- leave V to the total right of P_+ and in U_0^+ . Finally, all solutions starting in $V \setminus U^0$, between P_- and P_+ and above $\tilde{\Gamma}_{(\lambda, \varepsilon)}$ leave V in U_0^+ and to the total left of P_+ .

(iii) *For $\lambda \in (\lambda_{sc}, \lambda_0]$, all orbits starting in $V \setminus U^0$, leave V .*

(iv) *There exists some $\lambda_* \in (\lambda_H(\sqrt{\varepsilon}), \lambda_{sc}(\sqrt{\varepsilon}))$ such that for $\lambda < \lambda_*$, $U^0 \cap V_{2, \varepsilon}$ has width $\mathcal{O}(\varepsilon + \sqrt{\varepsilon}\lambda)$, while for $\lambda > \lambda_*$, $U^0 \cap V_{2, \varepsilon}$ has width of order $\mathcal{O}(\varepsilon^{3/2} + \sqrt{\varepsilon}\lambda)$. For all $\lambda \in [-\lambda_0, \lambda_0]$, $U^0 \cap V_{1, \varepsilon}$ has width of order $\mathcal{O}((u_\varepsilon(x))^2 + \lambda u_\varepsilon(x))$ for $(x, u_\varepsilon(x)) \in V_{1, \varepsilon}$.*

Remark 4.4. Note that the adaption of Theorem 3.2.iii to system (4.29)–(4.32) is more involved. Indeed, different phenomena can appear. One first naive idea for the corresponding behaviour would be the following:

(iii) For $\lambda \in (\lambda_c, \lambda_0]$ all orbits starting in $V \setminus U^0$ leave V in $V \setminus \mathcal{C}_0$ and to the total right of $\{(p_e^x, y) : y \in \mathbb{R}\}$.

This would reflect the fact that in the classical canard case, for $\lambda \in (\lambda_{sc}, \lambda_0]$, trajectories eventually end up on the right of the repelling slow manifold $\mathcal{C}_\varepsilon^r$ and are being repelled fast towards the right in (x, y) -phase space. However, it can happen that some solutions first spiral around the equilibrium p_e before this happens. In system (4.29)–(4.32), such solutions enter U_0^+ already before finishing the first half spiral and continue vertically upwards in U_0^+ until they leave V .

An extension of Theorem 4.3.iii is the following, see Figure 7

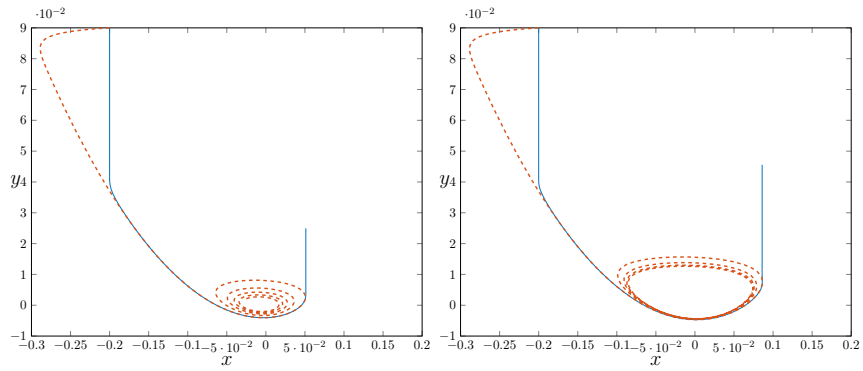
Theorem 4.5. *Suppose ε_0, λ_0 are sufficiently small and consider $V = V_{\varepsilon_0}$ as defined in Definition 1.1. Fix $\varepsilon \in (0, \varepsilon_0]$ and consider the notation from Theorems 4.2–4.3.*

For $\lambda \in (\lambda_c, \lambda_0]$, there exists a vertical line $P_c = P_{c,\lambda} = \{(p_c^x, y) : y \in \mathbb{R}\}$ such that the following holds true: All solutions starting in $V \setminus U^0$ and to the left of P_c leave V in $V \setminus \mathcal{C}_0$. All orbits starting in $\mathcal{C}_0 \setminus U^0$ and to the right of P_c leave V in U_0^+ .

Note that the set of solutions starting in $V \setminus U^0$ and to the left of P_c can be empty, since P_c can be located to the left of V .

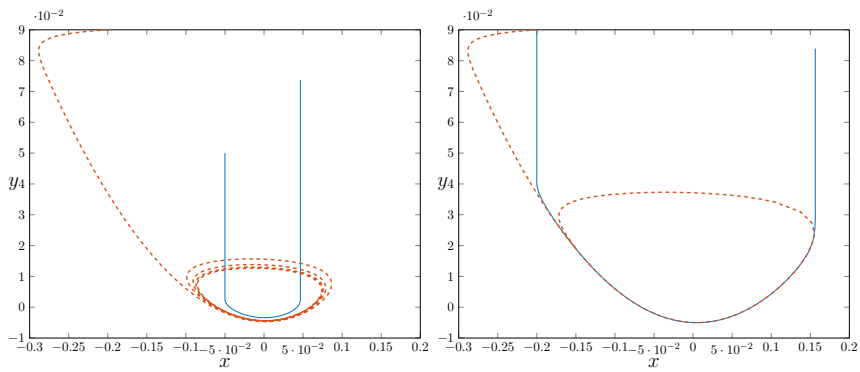
Remark 4.6. Note that in Theorem 4.5, among all trajectories starting to the right of P_c , besides orbits which leave V in U_0^+ , some solutions might leave V in $V \setminus \mathcal{C}_0$. This is why we have to restrict to orbits starting in $\mathcal{C}_0 \setminus U^0$, rather than considering initial conditions in the larger set $V \setminus U^0$.

Indeed, some orbits starting in $V \setminus \mathcal{C}_0$ and to the right of P_c correspond to orbits which spiral around p_e in the classical case since they are trapped by $\mathcal{C}_\varepsilon^r$, and some others are located below and to the right of $\mathcal{C}_\varepsilon^r$ and consequently move constantly to the right in (x, y) -phase space. In (4.29)–(4.32), orbits of the first kind leave V in U_0^+ , while orbits of the second kind leave V in $V \setminus \mathcal{C}_0$, see Figure 7.



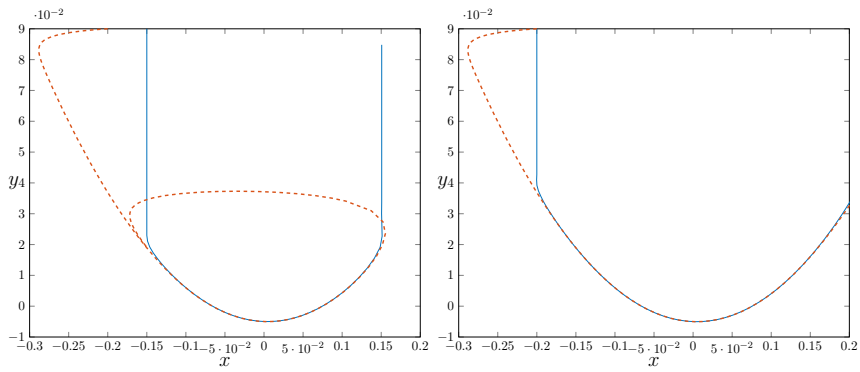
(a)

(b)



(c)

(d)



(e)

(f)

Figure 6: In this numerical example, $g = x(1+x)^{a_1} - g_2\lambda + g_3y$, with $a_1 = 1 = g_2$, $g_3 = a_2 = 0.9$ and $\varepsilon = 0.01$. In particular, $\lambda_H \approx \frac{-a_2}{2}\varepsilon = -4.5 \cdot 10^{-3} =: \lambda_{H,\text{appr}}$ and $\lambda_c \approx \frac{a_1 - a_2}{4}\varepsilon = 2.5 \cdot 10^{-4} =: \lambda_{c,\text{appr}}$. The value of λ increases along the pictures (a)-(f). In (a), $\lambda = 1.5 \cdot \lambda_{H,\text{appr}} < \lambda_H$, and we have an attracting equilibrium in the classical canard case (dashed line), while the trajectory enters \mathcal{C}_0 in U^+ in the non-smooth case (solid line). In (b),(c), $\lambda = 0.5 \cdot \lambda_{H,\text{appr}} > \lambda_H$, and we have a small attracting periodic orbit in the classical canard case (dashed line), while the trajectory enters \mathcal{C}_0 in U^+ in the non-smooth case (solid line). In (b), the trajectory for the non-smooth system starts above the exterior of the periodic orbit, while it starts above the interior of the periodic orbit in (c). As stated in Theorem 4.3, the trajectory leaves V to the right of the periodic orbit in (b), and the solution in (c) reenters \mathcal{C}_0 inside the orbit, i.e. it leaves V between P_-, P_+ . In (d)-(e), $\lambda = 0.2 \cdot \lambda_{c,\text{appr}} < \lambda_{sc}$, and we have a larger attracting periodic orbit in the classical canard case (dashed line), while the trajectory again reenters \mathcal{C}_0 in U^+ in the non-smooth case, but further to the right (solid line). Moreover, we observe the same relative positioning of the solution to the non-smooth system and the periodic orbit as in (b), (c). In (e), $\lambda = \lambda_{c,\text{appr}}$, and we obtain trajectories close to the maximal canard solution in the classical canard case (dashed line), as well as in the non-smooth case (solid line), once those solutions cross the parabola \mathcal{C}_∂ .

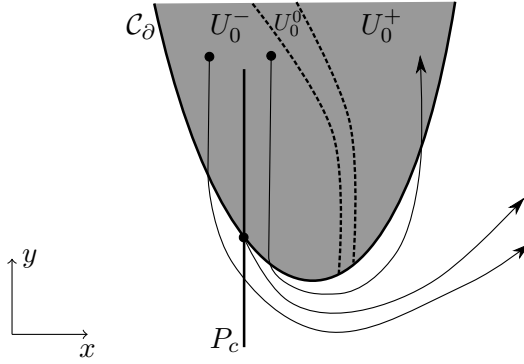


Figure 7: For $\lambda \in (\lambda_c(\sqrt{\varepsilon}), \lambda_0]$, all solutions starting in $P_c \cap \mathcal{C}_0$ leave V in $V \setminus \mathcal{C}_0$. In particular, this holds for the trajectory which starts at $(p_c^x, p_c^y) = P_c \cap \mathcal{C}_\partial$ (starting point in the middle). Trajectories starting in U_0^- (gray area left to the dashed lines) and to the left of P_c (left starting point) also leave V in $V \setminus \mathcal{C}_0$. Trajectories starting in U_0^- and to the right of P_c (right starting point) leave V in U_0^+ (gray area right of the dashed lines). The set $\{g = 0\} \cap \mathcal{C}_0$ is contained in U_0^0 (gray area between the dashed lines).

As for Theorems 3.1–3.2, we will show Theorems 4.2–4.5 with help of the weighted polar blow-up transformation Ψ as defined in (1.9) and the directional charts K_1 and K_2 according to (1.10)–(1.11). In particular, the desingularized vector field in chart K_1 is given by

$$x_1' = \begin{cases} -1 + x_1^2 - \frac{1}{2}\varepsilon_1 x_1 F(r_1, x_1, \varepsilon_1, \lambda_1), & \text{for } 1 < |x_1|, \\ -\frac{1}{2}\varepsilon_1 x_1 F(r_1, x_1, \varepsilon_1, \lambda_1), & \text{for } 1 \geq |x_1|, \end{cases} \quad (4.34)$$

$$r_1' = \frac{1}{2}r_1\varepsilon_1 F(r_1, x_1, \varepsilon_1, \lambda_1), \quad (4.35)$$

$$\varepsilon_1' = -\varepsilon_1^2 F(r_1, x_1, \varepsilon_1, \lambda_1), \quad (4.36)$$

$$\lambda_1' = -\frac{1}{2}\lambda_1\varepsilon_1 F(r_1, x_1, \varepsilon_1, \lambda_1), \quad (4.37)$$

where $F(r_1, x_1, \varepsilon_1, \lambda_1) = x_1 - \lambda_1 + r_1(a_1 x_1^2 + a_2) + \mathcal{O}(r_1(|r_1| + |\lambda_1|))$. Similarly, the desingularized vector field in the rescaling chart K_2 is given by

$$x_2' = \begin{cases} -y_2 + x_2^2, & \text{for } y_2 < x_2^2, \\ 0, & \text{for } y_2 \geq x_2^2, \end{cases} \quad (4.38)$$

$$y_2' = x_2 - \lambda_2 + r_2 G(x_2, y_2) + \mathcal{O}(r_2(|\lambda_2| + r_2)), \quad (4.39)$$

where $G(x_2, y_2) = a_1 x_2^2 + a_2 y_2$.

4.1 First chart

We analyze system (4.34)–(4.37) for $\lambda_1 \in (-\mu, \mu)$ with $\mu > 0$ small. In particular, for fixed ε , we prove that trajectories starting in $V_{1,\varepsilon}$ (see Section 1) and to the left of the set $U_{0,1}^1 = \Phi_1^{-1}(U_0^0, \varepsilon, \lambda) \cap V_1$ reach the domain $V_{2,\varepsilon}$ of transformation Φ_2 in finite time. On the other hand, solutions of system (4.34)–(4.37) which start to the right of $U_{0,1}^1$ move away from the canard point and from $V_{2,\varepsilon}$. Since system (4.34)–(4.37) is only piecewise smooth, we have to split $V_{1,\varepsilon}$ into the sets $\{x_1 < -1\}$, $\{-1 \leq x_1 < 0\}$, $\{0 < x_1 \leq 1\}$ and $\{1 < x_1\}$, and study the dynamics in each of these sets separately. Note that the hyperplanes $\{r_1 = 0\}$, $\{\varepsilon_1 = 0\}$ and $\{\lambda_1 = 0\}$ are invariant. Moreover, the line $l_1 = \{(x_1, 0, 0, 0) : x_1 \in \mathbb{R}\}$ contains the segment of equilibria $\{(x_1, 0, 0, 0) : x_1 \in [-1, 1]\}$, with endpoints $p_a = (-1, 0, 0, 0)$ and $p_r = (1, 0, 0, 0)$. For the flow on the line l_1 , p_a is attracting from the direction $x_1 < -1$ and p_r is repelling from $x_1 > 1$. The blown-up left branch of \mathcal{C}_∂ in chart K_1 is given by $\mathcal{C}_{0,1}^a = \{x_1 = -1, r_1 \geq 0\}$. Similarly, the right branch is given by $\mathcal{C}_{0,1}^r = \{x_1 = 1, r_1 \geq 0\}$.

Figure 8:

Projection to $\lambda_1 = \varepsilon_1 = 0$. Critical manifold $\mathcal{C}_{0,1}$ (gray) in chart K_1 with blown-up attracting branch $\mathcal{C}_{0,1}^a$ and blown-up repelling branch $\mathcal{C}_{0,1}^r$. Invariant line l_1 (dashed) with segment of equilibria $[p_a, p_r]$, where p_a is attracting from the left and p_r is repelling towards the right. The set $\{F = 0\} \cap \mathcal{C}_{0,1}$ is located in U_0^1 (area between the dashed curves).

In particular, the endpoints of $\mathcal{C}_{0,1}^a, \mathcal{C}_{0,1}^r$ are given by p_a and p_r respectively. In the invariant subset $\{\varepsilon_1 = 0 = \lambda_1\}$, the sets $\mathcal{C}_{0,1}^a, \mathcal{C}_{0,1}^r$ correspond to equilibria on the boundary of $\mathcal{C}_{0,1}$ of the reduced system

$$\begin{aligned} x_1' &= \begin{cases} -1 + x_1^2, & \text{for } 1 < |x_1|, \\ 0, & \text{for } 1 \geq |x_1|, \end{cases} \\ r_1' &= 0. \end{aligned}$$

The other equilibria of this reduced system are given by the set $\{(x_1, r_1, 0, 0) : |x_1| < 1, r_1 \geq 0\}$, i.e. by the projection of $\text{int}(\mathcal{C}_{0,1})$ to $\{\varepsilon_1 = 0 = \lambda_1\}$, see Figure 8. In the invariant subset $\{r_1 = 0 = \lambda_1\}$, the reduced system reads

$$\begin{aligned} x_1' &= \begin{cases} -1 + x_1^2 - \frac{1}{2}\varepsilon_1 x_1^2, & \text{for } 1 < |x_1|, \\ -\frac{1}{2}\varepsilon_1 x_1^2, & \text{for } 1 \geq |x_1|, \end{cases} \\ \varepsilon_1' &= -\varepsilon_1^2 x_1. \end{aligned}$$

The equilibria of this system are given by

$$\{(0, 0, \varepsilon_1, 0) : \varepsilon_1 \geq 0\} \cup \{(x_1, 0, 0, 0) : |x_1| \leq 1\},$$

and p_a, p_r are equilibria on the boundary of this set. Since λ_1, r_1 are small, $F(r_1, x_1, \varepsilon_1, \lambda_1) = x_1 - \lambda_1 + r_1(a_1x_1^2 + a_2) + \mathcal{O}(|r_1|(|r_1| + |\lambda_1|)) \neq 0$ for $|x_1|$ close to one. Therefore, $F \neq 0$ in the vicinity of p_a, p_r . In particular, $F < 0$ close to p_a and $F > 0$ close to p_r . Consider the smooth subsystems

$$\begin{cases} x_1' = -1 + x_1^2 - \frac{1}{2}\varepsilon_1x_1^2, \\ \varepsilon_1' = -\varepsilon_1^2x_1, \end{cases} \quad \begin{cases} x_1' = -\frac{1}{2}\varepsilon_1x_1^2, \\ \varepsilon_1' = -\varepsilon_1^2x_1. \end{cases}$$

For $p \in \{(0, 0, \varepsilon_1, 0), \varepsilon_1 \geq 0\} \cup \{(x_1, 0, 0, 0), |x_1| < 1\}$ we only have to consider the second subsystem since those equilibrium points are contained in the interior of the critical manifold. For all of these p , zero is the only eigenvalue of the (linearized) second subsystem. For the boundary equilibria p_a and p_r , zero is the only eigenvalue of the (linearized) second subsystem, which corresponds to perturbations in directions $x_1 > -1$ and $x_1 < 1$ respectively. For the (linearized) first subsystem, i.e. for directions $x_1 < -1$ and $x_1 > 1$ in the full system, both p_a and p_r have a triple zero eigenvalue with eigenvectors $(0, 1, 0, 0)$, $(0, 0, 0, 1)$, and $(1, 0, -2, 0)$ for p_a respectively $(1, 0, 2, 0)$ for p_r . Moreover, in the direction $x_1 < -1$, p_a has the eigenvalue -2 , while p_r has the eigenvalue 2 in the direction $x_1 > 1$, both with eigenvector $(1, 0, 0, 0)$. In the full system (4.34)–(4.37) also note that $x = r_1x_1$ remains constant in $\mathcal{C}_{0,1} = \{|x_1| \leq 1\}$ as a consequence of the second equation in (4.29). Similarly, $\varepsilon = r_1^2\varepsilon_1$ and $\lambda = r_1\lambda_1$ remain constant because of (4.31) and (4.32) respectively.

We can find some $C_1, C_2 > 0$ such that

$$\begin{aligned} U_1^1 := \{(x_1, r_1 + \tilde{r}_1, \lambda_1 + \tilde{\lambda}_1, \varepsilon_1) : x_1 - \lambda_1 + r_1(a_1x_1^2 + a_2) = 0, \\ |\tilde{r}_1| \leq C_1r_1^2, |\tilde{\lambda}_1\tilde{r}_1| \leq C_2|\lambda|\} \cap V_1 \end{aligned} \quad (4.40)$$

contains the set $\{F(x_1, r_1, \lambda_1, \varepsilon_1) = 0\} \cap V_1$ of roots of F . For $\lambda_1 \in [-\mu, \mu]$, $r_1 \in [-\rho, \rho]$ with μ, ρ small enough, the function $x_1 \mapsto -\frac{x_1 - \lambda_1}{a_1x_1^2 + a_2}$ is decreasing for $x_1 \in [-C_3, C_3]$ provided that $C_3 \in (0, 1)$ is small enough, while $-\frac{x_1 - \lambda_1}{a_1x_1^2 + a_2} > \rho$ for $|x_1| \in [C_3, x_{0,1}]$. Moreover, $-\frac{x_1 - \lambda_1}{a_1x_1^2 + a_2} > 0$ for $x_1 < -\lambda_1$. We introduce

$$\begin{aligned} U_1^- &:= \{F(x_1, r_1, \lambda_1, \varepsilon_1) < 0\} \setminus U_1^1, \\ U_1^+ &:= \{F(x_1, r_1, \lambda_1, \varepsilon_1) > 0\} \setminus U_1^1, \quad U_{0,1}^1 := U_1^1 \cap \mathcal{C}_{0,1}, \text{ and} \\ U_{0,1}^- &:= U_1^- \cap \mathcal{C}_{0,1}, \quad U_{0,1}^+ := U_1^+ \cap \mathcal{C}_{0,1}. \end{aligned} \quad (4.41)$$

Then the following lemma holds, see Figure 9:

Lemma 4.7. For ρ, μ small enough and $\varepsilon = r_1^2\varepsilon_1$, $\lambda = r_1\lambda_1$, we obtain the following types of trajectories for system (4.34)–(4.37):

- (i) For $(x_1(0), r_1(0), \lambda_1(0), \varepsilon_1(0)) \in U_1^- \setminus \mathcal{C}_{0,1}$, x_1 eventually reaches a small ball around -1 with $x_1 < -1$ and hence remains in $U_1^1 \setminus \mathcal{C}_{0,1}$. Moreover,

$$|r_1|' < 0, \quad \varepsilon_1' > 0, \quad \lambda_1' \operatorname{sgn}(\lambda_1(0)) > 0.$$

- (ii) For $(x_1(0), r_1(0), \lambda_1(0), \varepsilon_1(0)) \in U_{0,1}^-$ and $-1 \leq x_1(0) < 0$:

$$x_1 \downarrow -1, \quad r_1 \rightarrow -x_1(0)r_1(0), \quad \varepsilon_1 \uparrow \frac{\varepsilon}{r_1(0)^2 x_1(0)^2}, \quad \lambda_1 \rightarrow -\frac{\lambda}{r_1(0)x_1(0)},$$

as time increases. Moreover, these values are attained at a finite time $\tilde{t}_1 > 0$.

- (iii) For $(x_1(0), r_1(0), \lambda_1(0), \varepsilon_1(0)) \in U_{0,1}^+$, $r_1(0) \neq 0$ and $x_1(0) \leq 1$:

$$x_1 \downarrow \frac{r_1(0)x_1(0)}{\rho}, \quad |r_1| \uparrow \rho, \quad \varepsilon_1 \downarrow \frac{\varepsilon}{\rho^2}, \quad \lambda_1 \rightarrow \frac{\lambda}{\rho}, \quad \text{as } t_1 \text{ increases.}$$

- (iv) For $(x_1(0), r_1(0), \lambda_1(0), \varepsilon_1(0)) \in U_1^+ \setminus \mathcal{C}_{0,1}$:

$$x_1 \uparrow x_{1,0}, \quad |r_1| \uparrow \rho, \quad \varepsilon_1 \downarrow \frac{\varepsilon}{\rho^2}, \quad \lambda_1 \rightarrow \frac{\lambda}{\rho}, \quad \text{as } t_1 \text{ increases.}$$

Figure 9: Dynamics in Chart K_1 . The gray area depicts the projection of $\mathcal{C}_{0,1}$ to $\{\varepsilon_1 = 0\} \cup \{r_1 = 0\}$. The trajectories from left to right correspond to the cases (i)–(iv) in Lemma 4.7.

Proof. Statement i follows directly from the discussion above. For Statement ii, note that $x_1 \rightarrow -1$ as time increases because of the second equation in (4.34) and since $F < 0$, $x_1 < 0$ and $\varepsilon_1 > 0$ are bounded away from zero. Consequently, $x_1 = -1$ at a finite time $\tilde{t}_1 > 0$. Moreover, $x = r_1 x_1$, $\varepsilon = r_1^2 \varepsilon_1$ and $\lambda = r_1 \lambda_1$ remain constant as discussed above. This implies $r_1 \rightarrow -x_1(0)r_1(0)$, $\varepsilon_1 \rightarrow \frac{\varepsilon_1(0)r_1(0)^2}{r_1(0)^2 x_1(0)^2} = \frac{\varepsilon}{r_1(0)^2 x_1(0)^2}$ and $\lambda_1 \rightarrow -\frac{\lambda_1(0)r_1(0)}{r_1(0)x_1(0)} = -\frac{\lambda}{r_1(0)x_1(0)}$ for $t_1 \nearrow \tilde{t}_1$. Statements iii, iv are obtained similarly. \square

4.2 Second chart

In this subsection, we study the chart K_2 , i.e. (4.38)–(4.39):

$$x_2' = \begin{cases} -y_2 + x_2^2, & \text{for } y_2 < x_2^2, \\ 0, & \text{for } y_2 \geq x_2^2, \end{cases}$$

$$y_2' = x_2 - \lambda_2 + r_2(a_1 x_2^2 + a_2 y_2) + \mathcal{O}(r_2(|\lambda_2| + r_2)).$$

While the dynamics restricted to the critical manifold $\mathcal{C}_{0,2} = \{y_2 \geq x_2^2\}$ remains considerably easy, it turns out that solutions of (4.38)–(4.39) are obtained as small perturbations of constants of motion of the function $H(x_2, y_2) = \frac{1}{2} \exp(-2y_2) \left(y_2 - x_2^2 + \frac{1}{2}\right)$. To see this, consider the invariant subset $\{r_2 = 0 = \lambda_2\}$ and the reduced system

$$x_2' = \begin{cases} -y_2 + x_2^2, & \text{for } y_2 < x_2^2, \\ 0, & \text{for } y_2 \geq x_2^2, \end{cases} \quad (4.42)$$

$$y_2' = x_2. \quad (4.43)$$

Lemma 4.8. For system (4.42)–(4.43), we obtain the following:

- (i) For initial conditions of the form $x_2(0) = -c < 0$ and $y_2(0) > x_2(0)^2$, (x_2, y_2) reaches the point $(-c, c^2)$ after finite time with $x_2' = 0$, $y_2' = x_2 = -c$. From $(-c, c^2)$, (x_2, y_2) continues to the point (c, c^2) as a constant of motion of $H(x_2, y_2) = \frac{1}{4} \exp(-2c)$. Afterwards, $y_2 \rightarrow \infty$ as $t_2 \rightarrow \infty$ at speed $c > 0$, while $x_2 = c$ remains constant.
- (ii) For initial conditions of the form $x_2(0) = c > 0$ and $y_2(0) > x_2(0)^2$, $y_2 \rightarrow \infty$ as $t_2 \rightarrow \infty$ at speed $c > 0$, while $x_2 = c$ remains constant.
- (iii) The set $\mathbb{R}^2 \setminus \mathcal{C}_{0,2} = \{y_2 \leq x_2^2\}$ is invariant for all solutions of (4.42)–(4.43) with $H(x_2(0), y_2(0)) < 0$. In particular, each such solution is a constant of motion of H with $x_2 \rightarrow \infty$ as $t_2 \rightarrow \infty$.
- (iv) All equilibria of (4.42)–(4.43) are given by the half line $\{(0, y) : y \in \mathbb{R}^+\} \subset \mathcal{C}_{0,2}$.
- (v) The solution $\gamma_{c,2}(t_2) = \left(\frac{1}{2}t_2, \frac{1}{4}t_2^2 - \frac{1}{2}\right)$, $t_2 \in \mathbb{R}$, is a constant of motion for $H(x_2(0), y_2(0)) = 0$.

Proof. If $(x_2(0), y_2(0)) \in \{y_2 < x_2^2\}$, then (x_2, y_2) solves the system

$$\begin{aligned} x_2' &= -y_2 + x_2^2, \\ y_2' &= x_2. \end{aligned}$$

In particular, (x_2, y_2) is a constant of motion for the function $H(x_2, y_2) = \frac{1}{2} \exp(-2y_2) \left(y_2 - x_2^2 + \frac{1}{2}\right) = h$, until eventually $y_2 = x_2^2$. Note that trajectories with $h \leq 0$ satisfy $y_2 \leq x_2^2 - \frac{1}{2} < x_2^2$ at all times. Moreover, solutions with $h < 0$ correspond to unbounded solutions, which proves (iii). To see (v), note that the solution for $h = 0$ is given by

$$\gamma_{c,2}(t_2) = (x_{c,2}(t_2), y_{c,2}(t_2)) = \left(\frac{1}{2}t_2, \frac{1}{4}t_2^2 - \frac{1}{2}\right), \quad t_2 \in \mathbb{R}.$$

Moreover, $\frac{1}{4}$ is the global maximum of H and $H(x_2, y_2) = h \in \left(0, \frac{1}{4}\right]$ is satisfied for $y_2 = x_2^2 = c \geq 0$ if and only of

$$h = \frac{1}{2} \exp(-2c) \left(\frac{1}{2}\right) \Leftrightarrow c = c(h) := -\frac{1}{2} \log(4h) = -\log(2\sqrt{h}).$$

Here, $h = \frac{1}{4}$ corresponds to the equilibrium $(0, 0)$. Each trajectory with $h \in \left(0, \frac{1}{4}\right)$ and starting with $y_2 < x_2^2$ approaches the point $(\sqrt{c(h)}, c(h))$. In fact, for $y_2 < x_2^2$ and $x_2 < 0$, there hold $y_2' < 0$ and $x_2' > 0$, but since all constants of motion for H with $h \in \left(0, \frac{1}{4}\right)$ correspond to periodic orbits, $x_2' = 0 = -y_2 + x_2^2$ must hold at a certain time. This condition is only satisfied for the points $(\pm\sqrt{c(h)}, c(h))$, but (x_2^2, y_2) is moving away from the point $(-\sqrt{c(h)}, c(h))$ if the initial condition satisfies $y_2 < x_2^2$. This proves (ii), and (i) follows because $x_2' = 0, y_2' < 0$ hold for $y_2 > x_2^2, x_2 < 0$. Statement iv follows directly from (4.42)–(4.43). \square

With $\varepsilon = r_2^2, \lambda = r_2\lambda_2$, we can find $C_5 > 0$ such that the set

$$U_2^2 := \{(x_2, y_2 + \tilde{y}_2, r_2, \lambda_2) : x_2 - \lambda_2 + r_2(a_1x_2^2 + a_2y_2) = 0, \\ \tilde{x}_2 \in (-C_5(\varepsilon + |\lambda|), C_5(\varepsilon + |\lambda|))\} \cap V_2 \quad (4.44)$$

contains the set $\{g_2(x_2, y_2, r_2, \lambda_2) = 0\} \cap V_2$ of roots of g_2 , where

$$g_2(x_2, y_2, r_2, \lambda_2) = x_2 - \lambda_2 + r_2(a_1x_2^2 + a_2y_2) + \mathcal{O}(r_2(|\lambda_2| + r_2))$$

is the function on the right side of (4.39). The function $x_2 \rightarrow -\frac{x_2 - \lambda_2 + r_2a_1x_2^2}{a_2}$ is right-curved and decreasing for $x_2 > -\frac{1}{2a_1r_2}$. For $r_2 \in [-\rho, \rho]$ and ρ small enough, $x_2 > -\frac{1}{2a_1r_2}$ holds for all $(x_2, y_2) \in D$. Hence, for fixed r_2, λ_2 , the projection $P_{(x_2, y_2)}(U_2^2)$ into (x_2, y_2) -space has right-curved and decreasing boundaries. This implies that the projection $P_{(x_2, y_2)}(U_2^2)$ of U_2^2 into (x_2, y_2) -space splits \mathbb{R}^2 into the lower set $P_{(x_2, y_2)}(U_2^-)$, the separating set $P_{(x_2, y_2)}(U_2^2)$ and the upper set $P_{(x_2, y_2)}(U_2^+)$, where we define

$$\begin{aligned} U_2^- &:= \{g_2(x_2, y_2, r_2, \lambda_2) < 0\} \setminus U_2^2, \\ U_2^+ &:= \{g_2(x_2, y_2, r_2, \lambda_2) > 0\} \setminus U_2^2, \text{ and} \\ U_{0,2}^- &:= U_2^- \cap \mathcal{C}_0, \quad U_{0,2}^+ := U_2^+ \cap \mathcal{C}_0. \end{aligned} \quad (4.45)$$

4.3 Separation into Domains

With the notation of (4.40), (4.41), (4.44) and (4.45) we define

$$U^1 := P_{(x,y)}\Phi_1(U_1^1). \quad (4.46)$$

For $\lambda < \lambda_H$ we define

$$\begin{aligned} \tilde{U}_2^2 := \{ & (x_2, y_2 + \tilde{y}_2, r_2, \lambda_2) : x_2 - \lambda_2 + r_2(a_1x_2^2 + a_2y_2) = 0, \\ & \tilde{x}_2 \in (-C_6(\sqrt{\varepsilon} + |\lambda|), C_5(\varepsilon + |\lambda|))\} \cap V_2 \end{aligned} \quad (4.47)$$

for some appropriate $C_6 > 0$. For $\tilde{\Gamma}_{\lambda, \varepsilon, p_-, p_+}$ as introduced before Theorem 4.3, we can find some $\lambda_* > \lambda_H$ such that $p_+ \in P_{(x,y)}\Phi_2(U_2^2)$ for $\lambda \in (\lambda_H, \lambda_*)$ and $p_+ \notin P_{(x,y)}\Phi_2(U_2^2)$ for $\lambda \in [\lambda_*, \lambda_{sc}]$. We define

$$\begin{aligned} U^2 &:= P_{(x,y)}\Phi_2(\tilde{U}_2^2), \quad \text{for } \lambda \in [-\lambda_0, \lambda_*], \\ U^2 &:= P_{(x,y)}\Phi_2(U_2^2), \quad \text{for } \lambda \in [\lambda_*, \lambda_0]. \end{aligned} \quad (4.48)$$

Finally we set

$$U^0 := U^1 \cup U^2. \quad (4.49)$$

Moreover, we set

$$\begin{aligned} U^- &:= P_{(x,y)}(\Phi_1(U_1^-)) \cup [(P_{(x,y)}\Phi_2(U_2^-)) \setminus U^2], \\ U^+ &:= P_{(x,y)}(\Phi_1(U_1^+)) \cup [(P_{(x,y)}\Phi_2(U_2^+)) \setminus U^2], \end{aligned}$$

and

$$U_0^- := U^- \cap \mathcal{C}_0, \quad U_0^+ := U^+ \cap \mathcal{C}_0.$$

4.4 Proofs of the main results

Before we prove the main results, we study the relative positioning of $\mathcal{C}_\varepsilon^a$, $\mathcal{C}_\varepsilon^r$ and \mathcal{C}_0 .

Lemma 4.9. Consider the situation as in Theorems 4.2–4.5 and fix $\varepsilon \in (0, \varepsilon_0]$. Then the following statements hold for $\lambda \in (-\lambda_0, \lambda_{sc}(\sqrt{\varepsilon}))$:

- (i) Each trajectory starting in $U^- \setminus \mathcal{C}_0$ can only enter \mathcal{C}_0 in U_0^+ .
- (ii) The slow flow corresponding to $\mathcal{C}_\varepsilon^a$ enters V at $(p_\varepsilon^{a,x}, p_\varepsilon^{a,y}) \in \mathcal{C}_\varepsilon^a \cap \partial V$ with $p_\varepsilon^{a,x} < p_\varepsilon^x$ and there holds $(p_\varepsilon^{a,x}, p_\varepsilon^{a,y}) \in \mathbb{R}^2 \setminus \mathcal{C}_0$. The set $\mathcal{C}_\varepsilon^r \cap U^-$, where the corresponding slow flow leaves V , is located below $\mathcal{C}_\varepsilon^a$.
- (iii) The slow flow corresponding to $\mathcal{C}_\varepsilon^a$ enters \mathcal{C}_0 at $\mathcal{C}_\varepsilon^a \cap \mathcal{C}_\partial \in U_0^+$. For $\lambda \in (\lambda_H(\sqrt{\varepsilon}), \lambda_{sc}(\sqrt{\varepsilon}))$, this point is located to the right of P_+ .
- (iv) $\mathcal{C}_\varepsilon^r \cap \mathcal{C}_0$ is either empty or contained in U_0^+ and to the right of $\mathcal{C}_\varepsilon^a$.

Proof. (i) Let $(x(0), y(0))$ be located in $U^- \setminus \mathcal{C}_0$. Then by transformation to the chart K_1 or respectively K_2 , y is initially decreasing. Indeed, if $y(0) > 0$ we may apply the transformation to chart K_1 . By Lemma 4.7, $x_1(0) = \frac{x(0)}{\sqrt{y(0)}} < -1$ and $r_1 = \sqrt{y(0)} > 0$ imply that r_1 is initially decreasing until the solution enters V_{2,ρ^2} , where we can change into chart K_2 . Note that we still have $x_1 < -1$, $r_1 > 0$ at this time. In chart K_2 , we obtain $y_2 < x_2^2$ and $y_2 < -\frac{1}{r_2 a_2}(x_2 - \lambda_2 + r_2 a_1 x_2^2) + \mathcal{O}(|\lambda_2| + r_2)$. This implies that x_2 is increasing and y_2 decreasing. Moreover, U_2^2 has right-curved boundaries. If $\lambda \in (\lambda_*, \lambda_{sc}(\sqrt{\varepsilon}))$ then $p_+ \notin U^2$, and the trajectory can only reach the parabola in U^+ since it is attracted by $\tilde{\Gamma}_{(\lambda,\varepsilon)}$.

It remains to prove the statement for $\lambda \in [-\lambda_0, \lambda_*]$. We write $\mathcal{O}(2) := \mathcal{O}(r_2^2 + |r_2 \lambda_2| + \lambda_2^2)$ and consider $\lambda \in [-\lambda_0, \lambda_*]$. In order to prove the statement, it is enough to consider trajectories starting to the left of U_2^2 but close to p_e , and to prove that these trajectories reenter $\mathcal{C}_{0,2}$ to the right of U_2^2 . Hence, we consider trajectories with initial conditions of the form $x_2(0) = \lambda_2 - c$, $y_2(0) = (\lambda_2 - c)^2$, where $c = \mathcal{O}(r_2 + |\lambda_2|)$ and $c > \mathcal{C}_5(r_2^2 + r_2|\lambda_2|)$. We linearize (4.38)–(4.39) at $p_e = (\lambda_2, \lambda_2^2) + \mathcal{O}(2)$ to obtain

$$\begin{pmatrix} x_2 \\ y_2 \end{pmatrix}' = \begin{pmatrix} 2\lambda_2 & -1 \\ 1 & r_2 a_2 \end{pmatrix} \begin{pmatrix} x_2 - \lambda_2 \\ y_2 - \lambda_2^2 \end{pmatrix} + \mathcal{O}(2, (x_2 - \lambda_2)^2) =: A \begin{pmatrix} x_2 - \lambda_2 \\ y_2 - \lambda_2^2 \end{pmatrix} + \mathcal{O}(2, (x_2 - \lambda_2)^2).$$

Note that the higher order term $\mathcal{O}((x_2 - \lambda_2)^2)$ stems from the quadratic terms in x_2 in (4.38)–(4.39). In order to estimate trajectories of the full system, we study the linearized system

$$\begin{pmatrix} x \\ y \end{pmatrix}' = A \begin{pmatrix} x \\ y \end{pmatrix}.$$

We denote by (x, y) the solution of this system. Keep in mind that the term $(x_2(t) - \lambda_2)^2 = x(t)^2$ has to be of order $\mathcal{O}(2)$ until the trajectory reenters \mathcal{C}_0 , in order to ensure that (x_2, y_2) is approximated up to order $\mathcal{O}(2)$ by $(x + \lambda_2, y + \lambda_2^2) = (x, y) + p_e + \mathcal{O}(2)$. The eigenvalues of A are given by $\mu = \lambda_2 + \frac{r_2 a_2}{2} + i\frac{1}{2}\sqrt{|(2\lambda_2 - r_2 a_2)^2 - 4|}$ and $\bar{\mu}$. We abbreviate

$$k := \frac{1}{2}\sqrt{|(2\lambda_2 - r_2 a_2)^2 - 4|}.$$

The corresponding eigenvectors are given by

$$v = \begin{pmatrix} \lambda_2 - \frac{r_2 a_2}{2} + ik \\ 1 \end{pmatrix}$$

and \bar{v} respectively. Hence, we obtain real valued solutions of the linearized system as linear combinations of

$$e^{(\lambda_2 + \frac{r_2 a_2}{2})t} \begin{pmatrix} (\lambda_2 - \frac{r_2 a_2}{2}) \cos(kt) - k \sin(kt) \\ \cos(kt) \end{pmatrix},$$

$$e^{(\lambda_2 + \frac{r_2 a_2}{2})t} \begin{pmatrix} (\lambda_2 - \frac{r_2 a_2}{2}) \sin(kt) + k \cos(kt) \\ \sin(kt) \end{pmatrix}.$$

We want to estimate trajectories in (4.38)–(4.39) with initial conditions of the form $x_2(0) = \lambda_2 - c$, $y_2(0) = (\lambda_2 - c)^2$ for some $c > 0$. Hence, in the linearized system, we obtain initial conditions (up to order $\mathcal{O}(2)$) of the form $x(0) = -c$, $y(0) = -2\lambda_2 c + c^2 =: d$, and hence the solution

$$\begin{pmatrix} x(t) \\ y(t) \end{pmatrix} = e^{(\lambda_2 + \frac{r_2 a_2}{2})t} \left[\begin{pmatrix} -c \\ d \end{pmatrix} \cos(kt) - \begin{pmatrix} k^2 d + (\lambda_2 - \frac{r_2 a_2}{2})^2 d + (\lambda_2 - \frac{r_2 a_2}{2})c \\ (\lambda_2 - \frac{r_2 a_2}{2})d + c \end{pmatrix} \frac{\sin(kt)}{k} \right].$$

Note that the requirement $x(t)^2 = \mathcal{O}(2)$ is indeed fulfilled for $c = \mathcal{O}(r_2 + |\lambda_2|)$ and t bounded, since then $c^2 + |cd| + d^2 = \mathcal{O}(2)$. Also observe that $\frac{\sqrt{3}}{2} < k < 2$ for $\lambda_2 \in [-\mu, \lambda_{*,2}]$, where μ is small and with

$$\lambda_{H,2} = -\frac{r_2 a_2}{2} + \mathcal{O}(r_2^2) < \lambda_{*,2} < \mu.$$

For $c = \mathcal{O}(r_2 + |\lambda_2|)$ we obtain $d = \mathcal{O}(2)$ and therefore

$$\begin{pmatrix} x(t) \\ y(t) \end{pmatrix} = e^{(\lambda_2 + \frac{r_2 a_2}{2})t} \left[\begin{pmatrix} -c \\ 0 \end{pmatrix} \cos(kt) - \begin{pmatrix} 0 \\ c \end{pmatrix} \frac{\sin(kt)}{k} \right] + \mathcal{O}(2).$$

At this stage, in order to justify that (x_2, y_2) is indeed approximated up to order $\mathcal{O}(2)$ by $(\lambda_2 + x, \lambda_2^2 + y)$, it is crucial that x' and y' are not of order $\mathcal{O}(2)$ at the same time. This is satisfied if we require $c \neq \mathcal{O}(2)$. In this case, we obtain that - up to order $\mathcal{O}(2)$ - (x_2, y_2) reaches the parabola $\mathcal{C}_{\partial,2}$ at the first time $t > 0$ for which

$$\mathcal{O}(2) = -2\lambda_2 c e^{(\lambda_2 + \frac{r_2 a_2}{2})t} \cos(kt) + c^2 e^{2(\lambda_2 + \frac{r_2 a_2}{2})t} \cos^2(kt) = -\frac{c}{k} e^{(\lambda_2 + \frac{r_2 a_2}{2})t} \sin(kt).$$

Since $e^{(\lambda_2 + \frac{r_2 a_2}{2})t} = 1 + (\lambda_2 + \frac{r_2 a_2}{2})t + \mathcal{O}(2)$, we obtain

$$-\frac{c}{k} e^{(\lambda_2 + \frac{r_2 a_2}{2})t} \sin(kt) = -\frac{c}{k} \sin(kt) + \mathcal{O}(2).$$

Hence, this time is approximately given by $t = \frac{\pi}{k}$. But since

$$(x(\pi/k), y(\pi/k)) = (c, 0) + \mathcal{O}(2) = (c, c^2) + \mathcal{O}(2),$$

we obtain that (x_2, y_2) reaches the parabola at some point

$$(\lambda_2 + c, (\lambda_2 + c)^2) + \mathcal{O}(2).$$

If $C_7(r_2 + |\lambda_2|) \geq c \geq C_6(r_2 + r_2|\lambda_2|) > C_5(r_2^2 + r_2|\lambda_2|)$ (as in (4.47)) with appropriate $C_6, C_7 > 0$, then $c = \mathcal{O}(r_2 + |\lambda_2|)$ as required and at the same time $c \neq \mathcal{O}(2)$ as required. Moreover, the point $(c, c^2) + \mathcal{O}(2)$ is located in U_2^+ , which proves the statement for $\lambda \in [-\lambda_0, \lambda_*]$.

(ii) We will show in Lemma 4.10 that $\mathcal{C}_\varepsilon^a \cap (V \setminus V_{2,\varepsilon})$ is located below \mathcal{C}_0 , provided that ρ, λ_0 are small enough. Moreover, the slow flow corresponding to $\mathcal{C}_\varepsilon^a$ enters V at $(p_\varepsilon^{a,x}, p_\varepsilon^{a,y}) \in \mathcal{C}_\varepsilon^a \cap \partial V$ with $p_\varepsilon^{a,x} < p_e^x$. That $\mathcal{C}_\varepsilon^r \cap U^-$ is located below $\mathcal{C}_\varepsilon^a$ provided that $\lambda \in (-\lambda_0, \lambda_{sc}(\sqrt{\varepsilon}))$ is shown in [9].

(iii) By Theorem 3.1, in the classical case, the slow flow corresponding to $\mathcal{C}_\varepsilon^a$ is attracted to p_e for $\lambda \in (-\lambda_0, \lambda_H(\sqrt{\varepsilon})]$. For $\lambda \in (\lambda_H(\sqrt{\varepsilon}), \lambda_{sc}(\sqrt{\varepsilon}))$ it is attracted to $\Gamma_{\lambda,\varepsilon}$. Moreover, by (ii), $\mathcal{C}_\varepsilon^a$ can only be located outside of the periodic orbit. In both cases, this implies that the slow flow for $\mathcal{C}_\varepsilon^a$ enters \mathcal{C}_0 for the first time in U_0^+ . The corresponding solution of (4.29)–(4.32) remains in U_0^+ until it leaves V .

(iv) Follows from (ii) and (iii). \square

We are now able to prove the main results:

Proof of Theorem 4.2. That Γ_e exists follows from the implicit function theorem applied to (4.34)–(4.37) and (4.38)–(4.39). The existence of the values $\lambda_H(\sqrt{\varepsilon}) < \lambda_{sc}(\sqrt{\varepsilon})$ follows from Theorem 3.1. By Lemma 4.7, all trajectories starting in U_1^- , see (4.41), eventually reach the domain of definition of chart K_2 , either above or below the critical manifold, i.e. with $x_1 < -1$ close to -1 or still with $-1 < x_1 < 0$, but to the left of U^1 . Here, it is important to note that $U^1 = P_{(x,y)}\Phi_1(U_1^1)$ is right-curved so that $(x_1, r_1, \varepsilon_1, \lambda_1)$ never enters U_1^1 , see Lemma 4.7. Note also that U_1^- corresponds to the regions in (i) and (ii) of Lemma 4.7. By Lemma 4.9, the solution leaves the critical manifold at a point which is located above $\mathcal{C}_\varepsilon^a$, but reenters \mathcal{C}_0 in U_0^+ . Again by Lemma 4.9, this behaviour applies for all $\lambda \in (-\lambda_0, \lambda_{sc}(\sqrt{\varepsilon}))$.

A proof analog to that in [9] leads to the same results as in [9, Theorem 3.1] about the dependence on λ of the existence of a canard solution for the non-smooth problem (4.29)–(4.32). In particular, we obtain the expansion

$$\lambda_c(\sqrt{\varepsilon}) = -\left(\frac{a_2}{2} + \frac{-2a_1 - 2a_2}{8}\right)\varepsilon + \mathcal{O}(\varepsilon^{3/2}) = \frac{a_1 - a_2}{4}\varepsilon + \mathcal{O}(\varepsilon^{3/2})$$

for the critical value of λ which yields maximal canard solutions. Here, it is important to note that each maximal canard solution, restricted to V , is

strictly separated from \mathcal{C}_0 provided ρ, λ_0 are small enough. In particular, Lemma 4.10 shows that $\mathcal{C}_\varepsilon^a, \mathcal{C}_\varepsilon^r$ are located below \mathcal{C}_0 outside of $V_{2,\varepsilon}$. But inside $V_{2,\varepsilon}$, $\gamma_{c,2}$ lies strictly below $\mathcal{C}_{0,2}$, since $x_{c,2}^2 - y_{c,2} = \frac{1}{2}$. Because maximal canard solutions restricted to $V_{2,\varepsilon}$ are perturbations of $\gamma_{c,2}$ of order $\mathcal{O}(r_2, \lambda_2, r_2(|\lambda_2| + r_2))$, and since $r_2 = \sqrt{\varepsilon} \in [0, \rho)$, $\lambda_2 \in (-\mu, \mu)$, also this perturbation lies strictly below $\mathcal{C}_{0,2}$ for ρ, μ small. Finally, because maximal canard solutions are just the patching of $\mathcal{C}_\varepsilon^a, \mathcal{C}_\varepsilon^r$ restricted to $V \setminus V_{2,\varepsilon}$ and the perturbation of $\gamma_{c,2}$, this proves their existence and that their restriction to V is located below \mathcal{C}_0 . In particular, for $\lambda = \lambda_c(\sqrt{\varepsilon})$, the attracting slow manifold $\mathcal{C}_\varepsilon^a$ connects to $\mathcal{C}_\varepsilon^r$, and both are strictly separated from and located below \mathcal{C}_0 in V . \square

We prove the second main result:

Proof of Theorem 4.3. (i) follows from Theorem 4.2.

(ii) The first part of the statement follows from Theorem 3.1. Let $\lambda \in (\lambda_H(\sqrt{\varepsilon}), \lambda_{sc}(\sqrt{\varepsilon}))$. As in the proof of Theorem 4.2 consider any solution starting in U_0^- and to the left of P_- . This solution arrives at \mathcal{C}_∂ to the left of P_- and, by Lemma 4.9, above $\mathcal{C}_\varepsilon^a$. Since the trajectory behaves as a classical canard solution while contained in $\mathbb{R}^2 \setminus \mathcal{C}_0$, it remains between $\Gamma_{(\lambda,\varepsilon)}$ and $\mathcal{C}_\varepsilon^a$ until it reenters \mathcal{C}_0 to the right of P_+ . That the solution reenters \mathcal{C}_0 at all follows from Lemma 4.9. Now consider any solution starting in $V \setminus U^0$, between P_-, P_+ and above $\tilde{\Gamma}_{(\lambda,\varepsilon)}$. If the solution starts in U_0^- , then we can either apply the transformation to U_1^- , i.e. to chart K_1 , and use Lemma 4.7, or the transformation to chart K_2 and (4.38)–(4.39). In particular, the solution moves vertically downwards until it arrives at \mathcal{C}_∂ , still between P_-, P_+ and above $\tilde{\Gamma}_{(\lambda,\varepsilon)}$. Further on, the trajectory behaves as a classical canard solution and is - by Theorem 3.2 - attracted by $\tilde{\Gamma}_{(\lambda,\varepsilon)}$ from the interior, until it reenters \mathcal{C}_∂ in U_0^+ but to the left of P_+ .

(iii) As for $\lambda \in (-\lambda_0, \lambda_{sc}(\sqrt{\varepsilon}))$, one shows that Γ_e is unstable. Since there are no further equilibria contained in V , and because U^0 is right-curved, this proves the statement.

(iv) Follows from the definitions in Section 4.3. \square

Proof of Theorem 4.5. For $\lambda \in (\lambda_c(\sqrt{\varepsilon}), \lambda_0]$, considering the relative position of the attracting and the repelling slow manifold for the classical system (3.25)–(3.28) implies that $\mathcal{C}_\varepsilon^a$ does not intersect \mathcal{C}_∂ in V at all, see [9, 8] and Lemma 4.9 and the part of the proof of Theorem 4.2 about maximal canard solutions. In particular, $\mathcal{C}_\varepsilon^a \subset V \setminus \mathcal{C}_0$. Moreover, the repelling slow manifold in the classical case (in backward time) spirals around p_e until it eventually leaves V . For (4.29)–(4.32), this implies that there ex-

ists a unique point $(p_c^x, p_c^y) \in U_0^- \cap \mathcal{C}_\partial$ together with its vertical extension $P_c = \{(p_c^x, y) : y \in \mathbb{R}\}$ such that the following holds true:

The solution starting at (p_c^x, p_c^y) does not reenter \mathcal{C}_0 again. In particular, it leaves V in $V \setminus \mathcal{C}_0$. Moreover, all solutions starting in $U_0^- \cap \mathcal{C}_\partial$ and to the right of P_c reenter \mathcal{C}_0 in U_0^+ , see also Lemma 4.9.

This implies that all trajectories starting in $V \setminus U^0$ and to the left of P_c also leave V in $V \setminus \mathcal{C}_0$, since those trajectories stay to the left and below the solution starting at (p_c^x, p_c^y) .

Moreover, any solution starting in U_0^+ remains in this set until it leaves V , and any solution starting in U_0^- and to the right of P_c reaches \mathcal{C}_∂ to the right of P_c , so that it reenters \mathcal{C}_0 in U_0^+ , see Figure 7. \square

4.5 Slow manifold

In order to determine the dynamics of trajectories for (4.29)–(4.32), it is useful to know where there exist branches of the slow manifold which are separated from the critical manifold. That is, we want to know whether and where the attracting/repelling slow manifold of the smooth system (3.25)–(3.28) is located below the parabola $\mathcal{C}_\partial = \{(x, y) : y = x^2\}$. In particular, those branches $\mathcal{C}_\varepsilon^a$ and $\mathcal{C}_\varepsilon^r$ are still observed in system (4.29)–(4.32). However, also each trajectory in \mathcal{C}_0 follows the slow subsystem. This provides a key difference between system (3.25)–(3.28) with one-dimensional critical manifold \mathcal{C}_∂ and system (4.29)–(4.32) with critical manifold \mathcal{C}_0 of codimension zero. In this section, we study $\mathcal{C}_\varepsilon^a$ and $\mathcal{C}_\varepsilon^r$ outside the domain of K_2 , i.e. in sets of the form $\{(x, y) : y \in (\varepsilon, \rho^2), x \in (-x_{1,0}\sqrt{y}, x_{1,0}\sqrt{y})\}$, where Fenichel theory and asymptotic expansion techniques are applicable. In particular, we expand $x = x_{(0)} + \varepsilon x_{(1)} + \mathcal{O}(\varepsilon^2)$ and write $y = y(x)$. Then, we obtain due to (3.25)–(3.28) and the chain rule

$$\begin{aligned} \left(\frac{dx_{(0)}}{dy} + \varepsilon \frac{dx_{(1)}}{dy} + \mathcal{O}(\varepsilon^2) \right) \varepsilon g &= \frac{dx}{dy} \varepsilon g = \frac{dx}{dy} y' \\ &= x' = -y + x^2 = -y + x_{(0)}^2 + \varepsilon 2x_{(0)}x_{(1)} + \mathcal{O}(\varepsilon^2). \end{aligned}$$

Recall that $g = xg_1 - \lambda g_2 + yg_3$ is C^r -smooth for $r \geq 3$ and $g_i = g_i(x, y, \lambda)$ for $i = 1, 2, 3$, with $g_1, g_2 = 1 + \mathcal{O}(x, y, \lambda)$. Inserting the asymptotic expansion for x , we obtain by a Taylor expansion

$$\begin{aligned} g(x, y, \lambda) &= [g_1(0, 0, 0) + \partial_x g_1(0, 0, 0)(x_{(0)} + \varepsilon x_{(1)})](x_{(0)} + \varepsilon x_{(1)}) \\ &\quad - g_2(0, 0, 0)\lambda + g_3(0, 0, 0)y + \mathcal{O}(\varepsilon^2, xy, x\lambda, \lambda^2, y^2) \\ &= [1 + a_1(x_{(0)} + \varepsilon x_{(1)})](x_{(0)} + \varepsilon x_{(1)}) \\ &\quad - \lambda + a_2y + \mathcal{O}(\varepsilon^2, xy, x\lambda, \lambda^2, y^2) \\ &= x_{(0)} + a_1x_{(0)}^2 - \lambda + a_2y + \mathcal{O}(\varepsilon, xy, x\lambda, \lambda^2, y^2). \end{aligned}$$

Inserting this into the previous equation, sorting for terms of order $\mathcal{O}(1)$ and $\mathcal{O}(\varepsilon)$, and neglecting terms of order $\mathcal{O}(xy, x\lambda, \lambda^2, y^2)$ implies the conditions

$$y = x_{(0)}^2 \Leftrightarrow x_{(0)} = \pm\sqrt{y}, \quad \text{and then}$$

$$\pm\frac{1}{2\sqrt{y}}(\pm\sqrt{y} + (a_1 + a_2)y - \lambda) = \pm 2\sqrt{y}x_{(1)}.$$

Note here that $y > \varepsilon > 0$. Solving for $x_{(1)}$ yields

$$x_{(1)} = \frac{1}{4y}(\pm\sqrt{y} + (a_1 + a_2)y - \lambda).$$

Therefore,

$$x = x_{(0)} + \varepsilon x_{(1)} + \mathcal{O}(\varepsilon^2) = \begin{cases} -\sqrt{y} + \varepsilon\frac{1}{4y}(-\sqrt{y} + (a_1 + a_2)y - \lambda) \\ \sqrt{y} + \varepsilon\frac{1}{4y}(\sqrt{y} + (a_1 + a_2)y - \lambda) \end{cases} + \mathcal{O}(\varepsilon^2).$$

From this we obtain

$$\begin{aligned} x^2 &= \begin{cases} y - \varepsilon\frac{1}{2\sqrt{y}}(-\sqrt{y} + (a_1 + a_2)y - \lambda) \\ y + \varepsilon\frac{1}{2\sqrt{y}}(\sqrt{y} + (a_1 + a_2)y - \lambda) \end{cases} + \mathcal{O}(\varepsilon^2) \\ &= \begin{cases} y + \frac{\varepsilon}{2}\left(1 - (a_1 + a_2)\sqrt{y} + \frac{\lambda}{\sqrt{y}}\right) \\ y + \frac{\varepsilon}{2}\left(1 + (a_1 + a_2)\sqrt{y} - \frac{\lambda}{\sqrt{y}}\right) \end{cases} + \mathcal{O}(\varepsilon^2). \end{aligned}$$

In order to obtain branches of the slow manifold which are located below \mathcal{C}_∂ , we have to check if the conditions

$$C < \begin{cases} 1 - (a_1 + a_2)\sqrt{y} + \frac{\lambda}{\sqrt{y}}, \\ 1 + (a_1 + a_2)\sqrt{y} - \frac{\lambda}{\sqrt{y}}, \end{cases}$$

hold for some $C > 0$, since this implies that the $\mathcal{O}(\varepsilon)$ -terms are strictly positive and exceed the $\mathcal{O}(\varepsilon^2)$ -terms, provided that $\varepsilon \in (0, \rho^2]$ with ρ small enough. The first expression can be estimated from below by

$$1 - (a_1 + a_2)\sqrt{y} + \frac{\lambda}{\sqrt{y}} > 1 - (a_1 + a_2)\rho + \frac{\lambda}{\rho},$$

for $\varepsilon \in (0, \rho^2]$ and the right side is strictly larger than some $C > 0$ for $\lambda \in (-\lambda_0, \lambda_c]$, if $\rho, \lambda_0 > 0$ are chosen small enough. Similarly, the second expression can be estimated from below by

$$1 + (a_1 + a_2)\sqrt{y} - \frac{\lambda}{\sqrt{y}} > 1 + (a_1 + a_2)\sqrt{\varepsilon} - \frac{\lambda}{\sqrt{\varepsilon}},$$

and also this time the right side is strictly larger than some $C > 0$ for $\varepsilon \in (0, \rho^2]$ and $\lambda \in (-\lambda_0, \lambda_c]$, if $\rho, \lambda_0 > 0$ are chosen small enough. Note here, that $\lambda_c = \frac{a_1 - a_2}{4}\varepsilon + \mathcal{O}(\varepsilon^{3/2})$. In particular, this proves the following lemma.

Lemma 4.10. If $\rho, \lambda_0 > 0$ are chosen small enough, then for all $\varepsilon \in (0, \rho^2]$ and $\lambda \in (-\lambda_0, \lambda_c]$, the restrictions to $V \setminus V_{2,\varepsilon}$ of the attracting branch $\mathcal{C}_\varepsilon^a$ and the repelling branch $\mathcal{C}_\varepsilon^r$ of the slow manifold for system (3.25)–(3.28) are both located below the critical manifold \mathcal{C}_∂ . Here, $V = V_{\rho^2}$ is defined according to Definition 1.1.

Acknowledgments: This research was supported by the DFG Collaborative Research Center TRR109, Discretization in Geometry and Dynamics. CK would also like to thank the VolkswagenStiftung for support via a Lichtenberg Professorship.

References

- [1] E. Benoît, J.L. Callot, F. Diener, and M. Diener. Chasse au canards. *Collect. Math.*, 31:37–119, 1981.
- [2] M. Brokate and J. Sprekels. *Hysteresis and Phase Transitions*. Springer, 1996.
- [3] M. Desroches, E. Freire, S.J. Hogan, E. Ponce, and P. Thota. Canards in piecewise-linear systems: explosions and super-explosions. *Proc. R. Soc. A*, 469:20120603, 2013.
- [4] F. Dumortier. Techniques in the theory of local bifurcations: Blow-up, normal forms, nilpotent bifurcations, singular perturbations. In D. Schlomiuk, editor, *Bifurcations and Periodic Orbits of Vector Fields*, pages 19–73. Kluwer, Dordrecht, The Netherlands, 1993.
- [5] F. Dumortier and R. Roussarie. *Canard Cycles and Center Manifolds*, volume 121 of *Memoirs Amer. Math. Soc.* AMS, 1996.
- [6] N. Fenichel. Geometric singular perturbation theory for ordinary differential equations. *J. Differential Equat.*, 31:53–98, 1979.
- [7] C.K.R.T. Jones. Geometric singular perturbation theory. In *Dynamical Systems (Montecatini Terme, 1994)*, volume 1609 of *Lect. Notes Math.*, pages 44–118. Springer, 1995.
- [8] M. Krupa and P. Szmolyan. Extending geometric singular perturbation theory to nonhyperbolic points - fold and canard points in two dimensions. *SIAM J. Math. Anal.*, 33(2):286–314, 2001.
- [9] M. Krupa and P. Szmolyan. Relaxation oscillation and canard explosion. *J. Differential Equat.*, 174:312–368, 2001.

- [10] C. Kuehn. Scaling of saddle-node bifurcations: degeneracies and rapid quantitative changes. *J. Phys. A: Math. and Theor.*, 42(4):045101, 2009.
- [11] C. Kuehn. *Multiple Time Scale Dynamics*. Springer, 2015. 814 pp.
- [12] C. Kuehn and C. Münch. Generalized play hysteresis operators as limits of fast-slow systems. *SIAM J. Appl. Dyn. Syst.*, 16(3):1650–1685, 2017.
- [13] A. Mielke. Evolution of rate-independent systems. In C.M. Dafermos and E. Feireisl, editors, *Handbook of Differential Equations Evolutionary Equations*, volume 2, pages 461–559. North-Holland, 2005.
- [14] A. Mielke and T. Roubíček. *Rate-independent Systems*. Springer, 2015.
- [15] A. Roberts and P. Glendinning. Canard-like phenomena in piecewise-smooth Van der Pol systems. *Chaos*, 24(2):023138, 2014.
- [16] A. Visintin. *Differential Models of Hysteresis*. Springer, 1994.
- [17] S. Wiggins. *Normally Hyperbolic Invariant Manifolds in Dynamical Systems*. Springer, 1994.